Effect of Coriolis force on electrical conductivity tensor for the rotating hadron resonance gas

Nandita Padhan [1], Ashutosh Dwibedi [2], Arghya Chatterjee [1,*] and Sabyasachi Ghosh [2]
[1]*Department of Physics, National Institute of Technology Durgapur, Durgapur, 713209 West Bengal, India*
[2]*Department of Physics, Indian Institute of Technology Bhilai, Kutelabhata, Durg, 491001 Chhattisgarh, India*

(Received 27 March 2024; revised 21 June 2024; accepted 29 July 2024; published 12 August 2024)

We have investigated the influence of the Coriolis force on the electrical conductivity of hadronic matter formed in relativistic nuclear collisions, employing the hadron resonance gas model. A rotating matter in the peripheral heavy-ion collisions can be expected from the initial stage of quark matter to late-stage hadronic matter. Present work is focused on rotating hadronic matter, whose medium constituents—hadron resonances—can face a nonzero Coriolis force, which can influence the hadronic flow or conductivity. We estimate this conductivity tensor by using the relativistic Boltzmann transport equation. In the absence of Coriolis force, an isotropic conductivity tensor for hadronic matter is expected. However, our study finds that the presence of Coriolis force can generate an anisotropic conductivity tensor with three main conductivity components—parallel, perpendicular, and Hall—similarly to the effect of Lorentz force at a finite magnetic field. Our study has indicated that a noticeable anisotropy of conductivity tensor can be found within the phenomenological range of angular velocity $\Omega = 0.001$–0.02 GeV and hadronic scattering radius $a = 0.2$–2 fm.

DOI: 10.1103/PhysRevC.110.024904

I. INTRODUCTION

In off-central heavy-ion collision (HIC) experiments, a large orbital angular momentum (OAM) can be produced, and this initial OAM depends on factors such as system size, collision geometry, and collision energy, ranging from $10^3\hbar$ to $10^7\hbar$ [1–3]. After the collision, the spectators carry some of the angular momenta, and the rest is transferred to the produced quark-gluon matter. The initial OAM transferred to the medium is stored in the initial fluid velocity profile of the quark matter and at a later stage in the hadronic matter in the form of local vorticity. This OAM can induce various effects within the medium, like spin polarization, chiral vortical effect, etc. The vorticity leads to the alignment of hadrons along its direction, influenced by spin-orbit coupling. When considering all space-time points on the freeze-out hypersurface, local polarization accumulates, resulting in a global polarization aligned with the reaction plane or the angular momentum of the colliding nuclei. The global polarization of Λ and $\bar{\Lambda}$ particles has been measured by the STAR Collaboration in Au+Au collisions across a range of collision energies ($\sqrt{s_{NN}} = 7.7$–200 GeV), revealing a decreasing trend with collision energies [1]. Moreover, in the recent study with improved statistics at $\sqrt{s_{NN}} = 200$ GeV, a polarization dependence on the event-by-event charge asymmetry was observed, indicating a potential contribution to the global polarization from the axial current induced by the initial magnetic field [4]. Additionally, spin alignment has also been observed in vector mesons, with recent measurements conducted at Relativistic Heavy Ion Collider and Large Hadron Collider further contributing to our understanding of spin phenomena in heavy-ion collisions [5–7].

Now, from the theoretical direction, the effect of large OAM on the medium constituents has been studied even before the experimental work of STAR Collaboration [1] in the Refs. [2,3,8–14]. The experimental finding of global polarization of Λ and $\bar{\Lambda}$ particles in 2017 [1] also stimulated many theoretical investigations of vorticity and spin polarization effects in HIC [15–25]. The study of vorticity and the polarization of the particles produced by HICs has been done by multitude of theoretical approaches. References [26–42], with the help of covariant Wigner functions and quantum kinetic equations, have described the chiral effects and the spin polarization of final-state particles. On the other hand, the authors of Refs. [3,8–10,15,43–45] used the theory of relativistic statistical mechanics for a plasma in global equilibrium under rotation to describe the polarization of particles emitted from the kinetic freeze-out hypersurface. In contrast, in Refs. [2,11–14,46], the spin-orbit interaction in QCD has been used to describe the transfer of initial OAM density into the spin angular momentum, ultimately resulting in the spin polarization of particles. Moreover, the authors of Refs. [17–19,47–54] have developed a kinetic framework to establish the equations of spin hydrodynamics by including the spin tensor. In addition, several transport and hydrodynamical models [16,20–25,55–59] have also been used to estimate

*Contact author: achatterjee.phy@nitdgp.ac.in

spin polarization and vorticity results in HIC quantitatively. Thermodynamics of the hadronic medium under rotation have recently been explored by Refs. [60–62]. The phase structure of rigidly rotating plasma has been explored in Refs. [63,64]. The lattice quantum chromodynamics calculations in the presence of rotations can be found in the Refs. [65,66].

There is a similarity between magnetic field and rotation. The picture of Lorentz force in the presence of magnetic fields is quite similar to the picture of the Coriolis force in the presence of rotation. In Refs. [67–69], the equivalence between the Coriolis force and Lorentz force has been explored. In the presence of magnetic fields, the transport coefficients of the systems become anisotropic [70–83]. Accordingly, one should expect the anisotropic structure of the transport coefficients in a rotating frame due to the effect of the Coriolis force. In this paper, we will show how the electrical conductivity of the rotating hadronic matter formed in HIC can be modified in the presence of Coriolis force. In the papers [84,85], the authors have described how a rotating medium's shear viscosity and electrical conductivity become anisotropic in the presence of Coriolis force. Here we have extended the formalism of Ref. [85] from nonrelativistic to the relativistic case, which is applicable to calculate the electrical conductivity of the rotating hadronic matter. To fulfill this purpose, we employed the covariant Boltzmann transport equation (BTE) under the rotational background. In this framework, the space-dependent metric makes the connection coefficients nonzero, which in turn manifest themselves as the pseudo force terms in the covariant Boltzmann equation. To simplify the analysis, we ignored the quadratic and higher power of angular velocity Ω present in the covariant BTE. This simplification leads to the elimination of centrifugal effects and makes a seamless comparison possible with the magnetic field scenario. We modeled our rotating hadronic medium by resorting to the popular hadron resonance gas (HRG) model. This model is founded on principles derived from statistical mechanics of multihadron species. Using S-matrix calculation, it has been shown that in the presence of narrow resonances, the thermodynamics of the interacting gas of hadrons can be approximated by the ideal gas of hadrons and its resonances [86,87]. The HRG model has been extensively used to study thermodynamics [88,89] and conserved charge fluctuations [90–94], as well as transport coefficients [95–105], which are quite accepted for heavy-ion collision phenomenology. Recently, Refs. [71,72,78,79] have demonstrated the role of Lorentz force in creating anisotropic transportation of HRG system. However, the role of the Coriolis force in creating a similar kind of anisotropic transportation for the HRG system has not been studied yet, and here, we are first time going for this kind of investigation.

The article is arranged as follows: In Sec. II, we develop the necessary formalism needed for calculating electrical conductivity tensor in the presence of rotation. The master formula for hadronic matter with the HRG and QGP with massless approximation is provided in Secs. II A and II B from which the results are generated. In Sec. III, we present the numerical results with the plots of the variation of conductivity for QGP and hadronic matter both in the presence and absence of rotation. The article is summarised in Sec. IV.

II. FORMALISM

To begin with, let us briefly recapitulate the nonrelativistic kinetic model used to calculate the shear viscosity and electrical conductivity of the rotating nuclear matter in Refs. [84,85]. The nonrelativistic kinetic model consists of implementing the rotating coordinate transformation to break the particle velocity into two parts: (1) velocity $\vec{v}_r$ seen from a frame rotating with angular velocity $\vec{\Omega}$ and (2) a rigid rotor velocity $\vec{\Omega} \times \vec{r}$. Then, for the time evolution of the distribution function, the BTE is written down in the rotating frame (coordinates) with apparent or pseudo forces entering as the force terms. The transport properties are studied by expanding the solution to the BTE around the local equilibrium distribution in the rotating frame. In generalizing this model to the relativistic scenario, we will keep the same physical picture as that of its nonrelativistic counterpart. To carry out the relativistic extension in practice, we will obtain the equation of motion (EOM) and covariant BTE in a rotating frame with the help of rotating frame metric tensor $g_{\mu\nu}$ (not same as the flat metric $\eta_{\mu\nu}$) and connection coefficients $\Gamma^{\alpha}_{\mu\lambda}$ (vanishes in an inertial frame). As our relativistic kinetic model of rotating nuclear matter, let us consider a rotating system of hadrons moving with the momenta $\vec{p}_r$ (subscript r denotes hadron species; it should not be confused with radial coordinate).

The micro- and macroscopic expressions of current density for these collections of hadron resonances under an applied electric field $\vec{\tilde{E}} \equiv \tilde{E}\hat{e}$ are

$$J^i = \sum_r J^i_r = \sum_r g_r q_r \int \frac{d^3\vec{p}_r}{(2\pi)^3} \frac{p^i_r}{E_r} \delta f_r, \, (p_{r0} \equiv E_r), \quad (1)$$

$$J^i = \sum_r J^i_r = \sum_r \sigma^{ij}_r \tilde{E}_j \equiv \sigma^{ij} \tilde{E}_j, \quad (2)$$

where r is the label characterizing the different hadrons and resonances with charge q_r, energy E_r, momentum p_r, and degeneracy g_r. The δf_r quantifies the deviation of the system from local equilibrium. $J^i = \sum_r J^i_r$ and $\sigma^{ij} = \sum_r \sigma^{ij}_r$ are respectively the current density and conductivity tensor due to all the hadronic species comprised of baryons and mesons. The microscopic expression of current density in the HRG phase provided in Eq. (1) can be compared with the macroscopic expression $J^i = \sigma^{ij}\tilde{E}_j$ to obtain the conductivity tensor σ^{ij}. The deviation function δf_r written in Eq. (1) corresponds to the difference between the total distribution function and equilibrium distribution function for the rth hadronic species, i.e., $\delta f_r = f_r - f^0_r$. We will assume that the system is slightly out of equilibrium so that δf_r can be treated as a perturbation. The perturbation δf_r can be determined by using the BTE in a rotating frame. Before writing the BTE in the rotating frame, we will briefly address the rotating frame transformation and equation of motion of a hadron in a rotating frame. To analyze the hadronic medium rotating with an angular velocity $\vec{\Omega} \equiv \Omega\hat{\omega}$, we will make an explicit coordinate transformation from the inertial coordinates: (t, x, y, z) to the corotating

coordinates (t', x', y', z') as follows [63,64,106,107]:

$$\left.\begin{aligned} t' &= t \\ x' &= x\cos\Omega t + y\sin\Omega t \\ y' &= -x\sin\Omega t + y\cos\Omega t \\ z' &= z \end{aligned}\right\}, \tag{3}$$

where we assumed the angular velocity to be in the z direction, i.e., $\hat{\omega} = \hat{k}$. The squared differential length element ds^2 and the corotating frame metric $g^{\mu\nu}$ can be obtained from the Eq. (3) as [108–110]:

$$\begin{aligned} ds^2 &= g_{\mu\nu}dx'^{\mu}dx'^{\nu} = dt'^2(1-\Omega^2x'^2-\Omega^2y'^2) \\ &\quad + 2\Omega y'dt'dx' - 2\Omega x'dt'dy' - dx'^2 - dy'^2 - dz'^2, \\ g_{\mu\nu} &= \begin{pmatrix} 1-\Omega^2x'^2-\Omega^2y'^2 & \Omega y' & -\Omega x' & 0 \\ \Omega y' & -1 & 0 & 0 \\ -\Omega x' & 0 & -1 & 0 \\ 0 & 0 & 0 & -1 \end{pmatrix}. \end{aligned} \tag{4}$$

The connection coefficients $\Gamma^{\alpha}_{\mu\lambda}$ in corotating coordinates can be expressed in terms of the derivative of the metric tensor [111–113],

$$\Gamma^{\alpha}_{\mu\lambda} = \frac{1}{2}g^{\alpha\nu}\left(\frac{\partial g_{\nu\mu}}{\partial x^{\lambda}} + \frac{\partial g_{\lambda\nu}}{\partial x^{\mu}} - \frac{\partial g_{\mu\lambda}}{\partial x^{\nu}}\right), \tag{5}$$

where we dropped the overhead primes from the rotating frame variables. Since all the subsequent calculations will be performed from the rotating frame, we will drop the rotating frame quantities' overhead primes to simplify our notation. On explicit calculation with the help of Eq. (5), one finds that out of 64 components of $\Gamma^{\alpha}_{\mu\lambda}$ only six are nonzero [110]: $\Gamma^1_{00} = -\Omega^2 x$, $\Gamma^2_{00} = -\Omega^2 y$, $\Gamma^1_{20} = \Gamma^1_{02} = -\Omega$, $\Gamma^2_{10} = \Gamma^2_{01} = \Omega$. One can write down the EOM of a hadron in the rotating frame with the help of connection coefficients $\Gamma^{\alpha}_{\mu\lambda}$ as [111,112,114],

$$\frac{dp^{\alpha}}{d\tau} + \frac{1}{m}p^{\mu}p^{\lambda}\Gamma^{\alpha}_{\mu\lambda} = F^{\alpha}, \tag{6}$$

where p^{α}, F^{α}, and τ are the four-momentum, four-force, and proper time, respectively. To see the similarity between the EOM provided by Eq. (6) with the classical nonrelativistic EOM in the rotating frame [115,116], we rewrite Eq. (6) with the substitution of connection coefficients,

$$\frac{d\vec{p}}{dt} = \gamma_v m(\vec{\Omega}\times\vec{r})\times\vec{\Omega} + 2\gamma_v m(\vec{v}\times\vec{\Omega}), \tag{7}$$

where we employed $\gamma_v = \frac{dt}{d\tau}$, $p^{\alpha} = (\gamma_v m, \gamma_v m\vec{v}) = (\gamma_v m, \vec{p})$, and $F^{\alpha} = 0$. In comparison with the classical nonrelativistic EOM [115,116], we noticed that the first and second terms of the right-hand side of Eq. (7) correspond to centrifugal and Coriolis force with the extra multiplicative Lorentz factor γ_v. Moreover, comparing the Coriolis force expression $\vec{F}_{\rm Cor} = 2\gamma_v m(\vec{v}\times\vec{\Omega})$ established in Eq. (7) with the expression of Lorentz force $\vec{F}_{\rm Lor} = q(\vec{v}\times\vec{B})$, a direct equivalence can be obtained between the $\vec{\Omega}$ in the rotating frame and magnetic field $\vec{B}$ in the inertial frame. In the rotating frame with the metric tensor $g_{\mu\nu}$ the Lorentz factor γ_v can be expressed as [113,117]:

$$\gamma_v = \frac{1}{\sqrt{g_{00}\left(1+\frac{g_{0i}v^i}{g_{00}}\right)^2 - v^2}}, \tag{8}$$

where we used the definitions $v^i \equiv \frac{dx^i}{dt}$, $v^2 \equiv (\frac{g_{0i}g_{0j}}{g_{00}} - g_{ij})v^iv^j$. Similarly, one can easily show by using the relation $p^{\mu}p_{\mu} = p^{\mu}p^{\nu}g_{\mu\nu} = m^2$ and $p^0 = \frac{p_0 - g_{0i}p^i}{g_{00}}$ that [117–122],

$$p_0 = E = \sqrt{m^2g_{00} + (g_{0i}g_{0j} - g_{00}g_{ij})p^ip^j}. \tag{9}$$

Now, we will write down the BTE in the corotating frame variables by equating the variation of distribution function $f_r(x^{\mu}, \vec{p}_r)$ along the hadron's world line with the collision kernel $C[f_r]$ [118,123,124]:

$$\begin{aligned} m_r\frac{df_r(x^{\mu},\vec{p}_r)}{d\tau} &= C[f_r] \\ \Rightarrow m_r\frac{dx^{\mu}}{d\tau}\frac{\partial f_r}{\partial x^{\mu}} + m_r\frac{dp^i_r}{d\tau}\frac{\partial f_r}{\partial p^i_r} &= C[f_r] \\ \Rightarrow p^{\mu}_r\frac{\partial f_r}{\partial x^{\mu}} - \Gamma^i_{\mu\lambda}p^{\mu}_r p^{\lambda}_r\frac{\partial f_r}{\partial p^i_r} + m_rF^i_r\frac{\partial f_r}{\partial p^i_r} &= C[f_r], \end{aligned} \tag{10}$$

where we used the EOM provided in Eq. (6) to get the last step. Equation (10) can be easily written in a fully covariant manner as [118,123–125]:

$$p^{\mu}_r\frac{\partial f_r}{\partial x^{\mu}} - \Gamma^{\alpha}_{\mu\lambda}p^{\mu}_r p^{\lambda}_r\frac{\partial f_r}{\partial p^{\alpha}_r} + m_rF^{\alpha}_r\frac{\partial f_r}{\partial p^{\alpha}_r} = C[f_r], \tag{11}$$

where we treat f_r to be function of independent variables x^{α} and p^{α}_r, i.e., $f_r = f_r(x^{\alpha}, p^{\alpha})$. The four force F^{α} is the electromagnetic force, i.e., $F^{\alpha}_r = q_rF^{\alpha\beta}p_{r\beta}/m_r$, where $F^{\alpha\beta}$ is the Faraday tensor. In the above, we provided the covariant form of BTE, paying special attention to rotating coordinate transformation. Nevertheless, the arguments leading to the final form of BTE given in Eqs. (10) and (11) can be easily generalized for general coordinate transformation and gravity, with only notable changes appearing in the explicit expression metric tensor and connection coefficients [118,123–125]. The solution of Eq. (11) can be obtained by assuming the system to be slightly out of equilibrium so that we can write $f_r = f^0_r + \delta f_r$ with $f^0_r = 1/[e^{(p^{\alpha}_r u^{\beta}g_{\alpha\beta}-\mu)/T} - \xi] = 1/[e^{(p^{\alpha}_r u_{\alpha}-\mu)/T} - \xi]$, where $\xi = -1$ for baryons and $\xi = +1$ for mesons. The fluid velocity u^{μ} occurring in the equilibrium distributions f^0_r can be written as $u^{\mu} = \gamma_u(1, \vec{u})$, where

$$\gamma_u = \frac{1}{\sqrt{g_{00}\left(1+\frac{g_{0i}u^i}{g_{00}}\right)^2 - u^2}}, \left(u^2 \equiv \left(\frac{g_{0i}g_{0j}}{g_{00}} - g_{ij}\right)u^iu^j\right). \tag{12}$$

To simplify the analysis, we will approximate the collision term $C[f_r]$ by the expression given by relaxation

time approximation, i.e., $C[f_r] = -(u^\alpha p_\alpha)\frac{f_r - f_r^0}{\tau_c}$. Substituting $f_r = f_r^0 + \delta f_r$ in Eq. (11) we have

$$p_r^\mu \frac{\partial f_r^0}{\partial x^\mu} - \Gamma^\alpha_{\mu\lambda} p_r^\mu p_r^\lambda \frac{\partial}{\partial p_r^\alpha}\left(f_r^0 + \delta f_r\right) + q_r F^{\alpha\beta} p_{r\beta} \frac{\partial}{\partial p_r^\alpha}\left(f_r^0 + \delta f_r\right) = C[f_r] = -(u^\alpha p_\alpha)\frac{\delta f_r}{\tau_c}, \tag{13}$$

where we neglected space-time gradient of δf_r in the first term of Eq. (13) since it give rise to second-order gradient effects. The Faraday tensor $F^{\mu\nu}$ can be decomposed into electric $\tilde{E}^\mu$ and magnetic part $B^{\mu\nu}$ with the help of fluid velocity u^μ and projector $\Delta^{\mu\nu} = g^{\mu\nu} - u^\mu u^\nu$. We can write $F^{\mu\nu} = \tilde{E}^\mu u^\nu - \tilde{E}^\nu u^\mu + B^{\mu\nu}$, where $\tilde{E}^\mu \equiv F^{\mu\nu}u_\nu$ and $B^{\mu\nu} \equiv \Delta^\mu_\alpha F^{\alpha\beta}\Delta^\nu_\beta$. In the present article, we will focus only on the effect of the electric field; therefore, we will ignore the magnetic part $B^{\mu\nu}$ and rewrite Eq. (13) as

$$\left[p_r^\mu \frac{\partial f_r^0}{\partial x^\mu} - \Gamma^\alpha_{\mu\lambda} p_r^\mu p_r^\lambda \frac{\partial f_r^0}{\partial p_r^\alpha} + q_r p_{r\beta}(\tilde{E}^\alpha u^\beta - \tilde{E}^\beta u^\alpha)\frac{\partial f_r^0}{\partial p_r^\alpha}\right] - \Gamma^\alpha_{\mu\lambda} p_r^\mu p_r^\lambda \frac{\partial \delta f_r}{\partial p_r^\alpha} = -(u^\alpha p_\alpha)\frac{\delta f_r}{\tau_c}$$
$$\Rightarrow -f_r^0\left(1 + \xi f_r^0\right)\left[\frac{p_r^\mu p_r^\alpha}{T}(\partial_\mu u_\alpha - \Gamma^\sigma_{\mu\alpha} u_\sigma) + p_r^\mu (u_\alpha p_r^\alpha)\partial_\mu \frac{1}{T} - p_r^\mu \partial_\mu \frac{\mu}{T} - \frac{q_r \tilde{E}_\nu p_r^\nu}{T}\right]$$
$$- \Gamma^\sigma_{\mu\lambda} p^\mu p^\lambda \frac{\partial \delta f_r}{\partial p_r^\sigma} = -(u^\alpha p_\alpha)\frac{\delta f_r}{\tau_c}. \tag{14}$$

The first three terms in the square bracket of Eq. (14) give rise to viscous stresses and diffusion; they are related to the shear viscosity, bulk viscosity, and thermal conductivity of the hadronic medium. Since the present article is planned to calculate electrical conductivity, we will focus on the dissipative flow arising from the electric field. For the calculation of electrical conductivity Eq. (14) can be rewritten as

$$\frac{q_r f_r^0\left(1 + \xi f_r^0\right)}{T}\tilde{E}_\mu p^\mu - \Gamma^\sigma_{\mu\lambda} p^\mu p^\lambda \frac{\partial \delta f_r}{\partial p_r^\sigma} = -(u^\alpha p_\alpha)\frac{\delta f_r}{\tau_c}. \tag{15}$$

The explicit form of p_0 in the rotating frame can be written with the use of Eq. (4) in Eq. (9) as

$$p_0 = E = \sqrt{m^2(1-\Omega^2\rho^2) + (1-\Omega^2 x^2)(p^1)^2 + (1-\Omega^2 y^2)(p^2)^2 + (1-\Omega^2\rho^2)(p^3)^2 - 2\Omega^2 xy\, p^1 p^2}, \ (\rho \equiv x^2 + y^2). \tag{16}$$

Similarly, the contravariant time component of the momentum vector p^0 is given by

$$p^0 = \frac{p_0 + \vec{r}\cdot(\vec{p}\times\vec{\Omega})}{g_{00}}. \tag{17}$$

The invariant momentum space measure dP is given by

$$dP \equiv \sqrt{g}\frac{d^3p}{p_0}, \ \text{where } g \equiv -\det((g_{\mu\nu})). \tag{18}$$

In the rotating frame, $\det((g_{\mu\nu})) = -1$ and $dP = \frac{d^3p}{p_0} = \frac{d^3p}{E}$, which justifies the invariant momentum measure in our original definition in Eq. (1). At this juncture, it should be pointed out that, in principle, one can solve Eq. (15) to obtain the electrical conductivity of rotating HRG without resorting to any further approximation. Nevertheless, the result becomes algebraically convoluted because of the space-dependent metric $g_{\mu\nu}$, which significantly differs from the flat metric $\eta_{\mu\nu}$. As the beginning level of calculation for our relativistic kinetic model of rotating matter, we will rely on two different approximations. These two approximations will simplify our result and make a seamless comparison with the magnetic field scenario possible. The first phase of approximation assumes that globally rotating nuclear matter is produced in HIC by ignoring radial expansion. This implies the fluid velocity $u^\mu = \gamma_u(1, \vec{u}) \xrightarrow{u^i=0} (\frac{1}{\sqrt{g_{00}}}, 0)$, in the globally comoving frame. Similarly, the local equilibrium distribution and electric field can be written as $f_r^0 = 1/[e^{(p_{r\alpha}u^\alpha - \mu)/T} - \xi] \xrightarrow{u^i=0} 1/[e^{(p_{r0}/\sqrt{g_{00}} - \mu)/T} - \xi]$ and $\tilde{E}_\nu = F_{\nu\mu}u^\mu \xrightarrow{u^i=0} F_{\nu 0}/\sqrt{g_{00}} = -\tilde{E}^i/\sqrt{g_{00}}$. Equation (15) in the comoving frame becomes

$$-\frac{f^0(1+\xi f^0)}{T}\frac{q}{\sqrt{g_{00}}}\vec{\tilde{E}}\cdot\vec{p} + 2p^0(\vec{p}\times\vec{\Omega})\cdot\frac{\partial\delta f}{\partial\vec{p}} + (p^0)^2((\vec{\Omega}\times\vec{r})\times\vec{\Omega})\cdot\frac{\partial\delta f}{\partial\vec{p}} = -\frac{p_0}{\sqrt{g_{00}}}\frac{\delta f}{\tau_c}$$
$$\Rightarrow -\frac{f^0(1+\xi f^0)}{T}\frac{q\vec{\tilde{E}}\cdot\vec{p}}{p_0} + \frac{2p^0\sqrt{g_{00}}(\vec{p}\times\vec{\Omega})}{p_0}\cdot\frac{\partial\delta f}{\partial\vec{p}} + \frac{(p^0)^2\sqrt{g_{00}}}{p_0}((\vec{\Omega}\times\vec{r})\times\vec{\Omega})\cdot\frac{\partial\delta f}{\partial\vec{p}} = -\frac{\delta f}{\tau_c}, \tag{19}$$

where we have suppressed the index r in writing Eq. (19), which will be retained during the calculation of total conductivity. The second phase of approximations will be implemented in solving Eq. (19) with the help of the ansatz $\delta f = -\vec{p}\cdot\vec{X}(\frac{\partial f^0}{\partial E}) = \vec{p}\cdot\vec{X}\frac{f^0(1+\xi f^0)}{T}$, where $\vec{X}$ is still to be determined. This approximation includes the following: Ωx, Ωy, and $\frac{\Omega}{T}$ are small, so one

can ignore the second- or higher-order terms containing products of any two of them. Neglecting the quadratic terms in Ωx and/or Ωy in Eq. (16) we have $p_0 = \sqrt{m^2 + \vec{p}^2}$. Employing the above approximation, the Coriolis force term in Eq. (19) can be written as

$$\frac{2p^0\sqrt{g_{00}}(\vec{p}\times\vec{\Omega})}{p_0}\cdot\frac{\partial\delta f}{\partial\vec{p}} = \frac{2}{p_0\sqrt{g_{00}}}[p_0 + \vec{r}\cdot(\vec{p}\times\vec{\Omega})](\vec{p}\times\vec{\Omega})\cdot\frac{\partial\delta f}{\partial\vec{p}}$$
$$\Rightarrow \frac{2p^0\sqrt{g_{00}}(\vec{p}\times\vec{\Omega})}{p_0}\cdot\frac{\partial\delta f}{\partial\vec{p}} \approx 2(\vec{p}\times\vec{\Omega})\cdot\frac{\partial\delta f}{\partial\vec{p}}, (g_{00} = 1-\Omega(x^2+y^2)\approx 1). \tag{20}$$

Similarly, it can be easily checked that the centrifugal force term $\frac{(p^0)^2\sqrt{g_{00}}}{p_0}((\vec{\Omega}\times\vec{r})\times\vec{\Omega})\cdot\frac{\partial\delta f}{\partial\vec{p}}$ completely drops out, leaving the following equation to be solved:

$$\frac{\partial f^0}{\partial E}\frac{\vec{p}}{p_0}\cdot(q\vec{\tilde{E}}) + 2m\gamma_v(\vec{v}\times\vec{\Omega})\cdot\frac{\partial\delta f}{\partial\vec{p}} = -\frac{\delta f}{\tau_c}. \tag{21}$$

One has to solve Eq. (21) for δf to determine HRG current density J^i from Eq. (1). So everything boils down to the determination of $\vec{X}$ in the ansatz: $\delta f = -\vec{p}\cdot\vec{X}(\frac{\partial f^0}{\partial E})$. Our system of rotating HRG is no longer isotropic because of the presence of the angular velocity vector $\vec{\Omega} = \Omega\hat{\omega}$. We have two unit vectors $\hat{\omega}$ and $\hat{e}$ in our hand, which can be used to construct another unit vector $\hat{e}\times\hat{\omega}$ perpendicular to both $\hat{\omega}$ and $\hat{e}$. In general, the current density in rotating HRG can have components along $\hat{\omega}$, $\hat{e}$, and $\hat{e}\times\hat{\omega}$. Since the vector $\vec{X}$ determines the form of the current density through Eq. (1), we can guess the following decomposition of $\vec{X} = \alpha\hat{e} + \beta\hat{\omega} + \gamma(\hat{e}\times\hat{\omega})$ with the unknowns α, β, and γ. The mathematical steps for the calculation of α, β, and γ and the subsequent determination of current density runs exactly similar to the nonrelativistic calculation done in Ref. [85]. Therefore, the main results will be written here, and a detailed calculation will be carried out in the Appendix A 1. The total conductivity for the rotating HRG derived in Appendix A 1 is given by

$$\sigma^{ij} = \sigma^0\delta_{ij} + \sigma^1\epsilon_{ijk}\omega_k + \sigma^2\omega_i\omega_j,$$
$$\text{with}\quad \sigma^n = \sum_r\frac{g_r q_r^2}{3T}\int\frac{d^3p}{(2\pi)^3}\frac{\tau_c\left(\frac{\tau_c}{\tau_\Omega}\right)^n}{1+\left(\frac{\tau_c}{\tau_\Omega}\right)^2}\times\frac{p^2}{E^2}f_r^0\left(1+\xi f_r^0\right). \tag{22}$$

For the angular velocity in the z direction, i.e., $\vec{\Omega} = \Omega\hat{k}$, the conductivity matrix has the following form,

$$[\sigma] = \begin{pmatrix}\sigma^0 & \sigma^1 & 0\\ -\sigma^1 & \sigma^0 & 0\\ 0 & 0 & \sigma^0+\sigma^2\end{pmatrix}. \tag{23}$$

A. Electrical conductivity for HRG

A quick glance at the matrix in Eq. (23) led us to define the following conductivity components: parallel conductivity (parallel to angular velocity $\vec{\Omega}$) $\sigma^{||} \equiv \sigma^0 + \sigma^2$, perpendicular conductivity (perpendicular to angular velocity $\vec{\Omega}$) $\sigma^{\perp} \equiv \sigma^0$, and cross- or Hall-like conductivity $\sigma^{\times} \equiv \sigma^1$. Moreover, one can identify $\sigma_{||}$ with the conductivity in the absence of Ω, i.e., $\sigma^{||} \equiv \sigma$.

In Eq. (22), we have derived the conductivity tensor for the rotating hadron gas. We can rewrite this equation with two separate summations for the baryons and mesons, respectively, along with their spin degeneracy factors. The parallel conductivity of the rotating HRG (or the HRG conductivity in the absence of Ω) at $\mu = 0$ is given by

$$\sigma^{||}_{\rm HRG} \equiv \sigma_{\rm HRG} = \sum_B\frac{g_B q_B^2}{3T}\int\frac{d^3p}{(2\pi)^3}\tau_c\times\frac{p^2}{E^2}f^0(1-f^0)$$
$$+\sum_M\frac{g_M q_M^2}{3T}\int\frac{d^3p}{(2\pi)^3}\tau_c\times\frac{p^2}{E^2}f^0(1+f^0), \tag{24}$$

where g_H is spin degeneracy of hadrons with charges q_H, masses m_H, and energy $E = \sqrt{p^2+m_H^2}$. For $H =$ mesons and baryons, equilibrium distribution function will be $f_0 = \frac{1}{e^{E/T}-1}$ and $f_0 = \frac{1}{e^{E/T}+1}$, respectively. Hadrons with a neutral electric charge will not participate in electrical conductivity.

The relaxation time of any hadron can be written as

$$\tau_c = 1/(n_{\rm HRG}v_{\rm av}^H\pi a^2), \tag{25}$$

where hard-sphere cross section πa^2 is considered for hadron, having average velocity

$$v_{\rm av}^H = \int\frac{d^3p}{(2\pi)^3}\frac{p}{E}f_0\Big/\int\frac{d^3p}{(2\pi)^3}f_0. \tag{26}$$

Each hadron will face the entire density of the system,

$$n_{\rm HRG} = \sum_B g_B\int_0^\infty\frac{d^3p}{(2\pi)^3}\frac{1}{e^{E/T}+1}$$
$$+\sum_M g_M\int_0^\infty\frac{d^3p}{(2\pi)^3}\frac{1}{e^{E/T}-1}, \tag{27}$$

where g_B and g_M are baryon and meson spin degeneracy factors, respectively.

The perpendicular electrical conductivity of the rotating HRG can be written as

$$\sigma^{\perp}_{\rm HRG} = \sum_B\frac{g_B q_B^2}{3T}\int\frac{d^3p}{(2\pi)^3}\frac{\tau_c}{1+\left(\frac{\tau_c}{\tau_\Omega}\right)^2}\times\frac{p^2}{E^2}f^0(1-f^0)$$
$$+\sum_M\frac{g_M q_M^2}{3T}\int\frac{d^3p}{(2\pi)^3}\frac{\tau_c}{1+\left(\frac{\tau_c}{\tau_\Omega}\right)^2}\times\frac{p^2}{E^2}f^0(1+f^0). \tag{28}$$

Similarly, the Hall electrical conductivity can be expressed as

$$\sigma^{\times}_{\rm HRG} = \sum_B \frac{g_B q_B^2}{3T}\int \frac{d^3p}{(2\pi)^3}\frac{\tau_c\left(\frac{\tau_c}{\tau_\Omega}\right)}{1+\left(\frac{\tau_c}{\tau_\Omega}\right)^2}\times\frac{p^2}{E^2}f^0(1-f^0)+\sum_M \frac{g_M q_M^2}{3T}\int \frac{d^3p}{(2\pi)^3}\frac{\tau_c\left(\frac{\tau_c}{\tau_\Omega}\right)}{1+\left(\frac{\tau_c}{\tau_\Omega}\right)^2}\times\frac{p^2}{E^2}f^0(1+f^0). \tag{29}$$

B. Electrical conductivity for mass-less QGP

We can construct the conductivity tensor for the massless rotating QGP by substituting $p = E$ in Eq. (22) and summing over all the light quarks with their corresponding degeneracies as

$$\begin{aligned}
\sigma^n_{\rm QGP} &= \sum_{f=u,d,s}\frac{g_f q_f^2}{6\pi^2 T}\frac{\tau_c\left(\frac{\tau_c}{\tau_\Omega}\right)^n}{1+\left(\frac{\tau_c}{\tau_\Omega}\right)^2}\int dE E^2 f^0(1-f^0)\\
&= \sum_{f=u,d,s}\frac{g_f q_f^2}{6\pi^2 T}\frac{\tau_c\left(\frac{\tau_c}{\tau_\Omega}\right)^n}{1+\left(\frac{\tau_c}{\tau_\Omega}\right)^2}T\frac{\partial}{\partial\mu}\int dE E^2 f^0\\
&= \sum_{f=u,d,s}\frac{g_f q_f^2}{6\pi^2 T}\frac{\tau_c\left(\frac{\tau_c}{\tau_\Omega}\right)^n}{1+\left(\frac{\tau_c}{\tau_\Omega}\right)^2}T\frac{\partial}{\partial\mu}T^3\Gamma(3)f_3(A) \quad \left[\text{where } f_j(A)=\frac{1}{\Gamma(j)}\int_0^\infty \frac{x^{j-1}dx}{A^{-1}e^x+1},\ (A\equiv e^{\mu/T})\right]\\
&= \sum_{f=u,d,s}\frac{g_f q_f^2}{6\pi^2 T}\frac{\tau_c\left(\frac{\tau_c}{\tau_\Omega}\right)^n}{1+\left(\frac{\tau_c}{\tau_\Omega}\right)^2}T\frac{\partial}{\partial\mu}T^3\Gamma(3)f_3(A)\\
&= \sum_{f=u,d,s}\frac{g_f q_f^2}{3\pi^2}\frac{\tau_c\left(\frac{\tau_c}{\tau_\Omega}\right)^n}{1+\left(\frac{\tau_c}{\tau_\Omega}\right)^2}T^2 f_2(A).
\end{aligned} \tag{30}$$

The electrical conductivity for massless QGP in the absence of rotation (or parallel conductivity of rotating QGP) is defined as,

$$\begin{aligned}
\sigma_{\rm QGP} \equiv \sigma^{||}_{\rm QGP} = \sigma^0_{\rm QGP} + \sigma^2_{\rm QGP} &= \frac{1}{3\pi^2}\left(\sum_{f=u,d,s} g_f q_f^2\right)\tau_c T^2 L_2\\
&= \frac{8e^2}{3\pi^2}\tau_c T^2 L_2,
\end{aligned} \tag{31}$$

where g_f = spin degeneracy × color degeneracy × particle-antiparticle degeneracy= $2\times3\times2=12$ for any quark flavor $f = u, d, s$ with charges $q_u = +\frac{2}{3}e$, $q_d = -\frac{1}{3}e$, $q_s = -\frac{1}{3}e$. In natural unit $e^2 = 4\pi/137$. Being electric charge neutral, gluons will not participate in electrical conductivity. At $\mu = 0$, Fermi integral function f_n will convert to L_n:

$$L_j = \frac{1}{\Gamma(j)}\int_0^\infty \frac{x^{j-1}dx}{e^x+1} = f_j(1), \tag{32}$$

where we have chosen $\xi = -1$, since quarks are fermions.

Now quarks will face the entire QGP density

$$\begin{aligned}
n_{\rm QGP} &= g_q\int_0^\infty \frac{d^3p}{(2\pi)^3}\frac{1}{e^{p/T}+1} + g_g\int_0^\infty \frac{d^3p}{(2\pi)^3}\frac{1}{e^{p/T}-1}\\
&= \left[g_q\left(1-\frac{1}{2^{3-1}}\right)+g_g\right]\frac{\zeta(3)}{\pi^2}T^3,\\
&= \left[\frac{3g_q}{4}+g_g\right]\frac{\zeta(3)}{\pi^2}T^3,
\end{aligned} \tag{33}$$

where $g_q = 2\times3\times2\times3 = 36$ and $g_g = 2\times8 = 16$ are quark and gluon degeneracy factors respectively and Reimann zeta function $\zeta(3) = 1.202$.

One can write perpendicular electrical conductivity $\sigma^{\perp} \equiv \sigma^0$ for rotating QGP from Eq. (30) as

$$\begin{aligned}
\sigma^{\perp}_{\rm QGP} &= \frac{1}{3\pi^2}\left(\sum_{f=u,d,s} g_f q_f^2\right)\frac{\tau_c}{1+\left(\frac{\tau_c}{\tau_\Omega}\right)^2}T^2 L_2\\
&= \frac{8e^2}{3\pi^2}\frac{\tau_c}{1+\left(\frac{\tau_c}{\tau_\Omega}\right)^2}T^2 L_2.
\end{aligned} \tag{34}$$

Similarly, from Eq. (30) the Hall electrical conductivity $\sigma^{\times} \equiv \sigma^1$ can be expressed as

$$\begin{aligned}
\sigma^{\times}_{\rm QGP} &= \frac{1}{3\pi^2}\left(\sum_{f=u,d,s} g_f q_f^2\right)\frac{\tau_c\left(\frac{\tau_c}{\tau_\Omega}\right)}{1+\left(\frac{\tau_c}{\tau_\Omega}\right)^2}T^2 L_2\\
&= \frac{8e^2}{3\pi^2}\frac{\tau_c\left(\frac{\tau_c}{\tau_\Omega}\right)}{1+\left(\frac{\tau_c}{\tau_\Omega}\right)^2}T^2 L_2.
\end{aligned} \tag{35}$$

III. RESULTS AND DISCUSSION

For numerical evaluation of electrical conductivities for a rotating QGP, we have employed the formulas put down in Sec. II B. Similarly, for quantitative estimation of electrical conductivities for the rotating hadron gas, we use the ideal hadron resonance gas model established in Sec. II A, which encompasses all the noninteracting hadrons and their resonance particles up to a mass of 2.6 GeV as listed in Ref. [126].

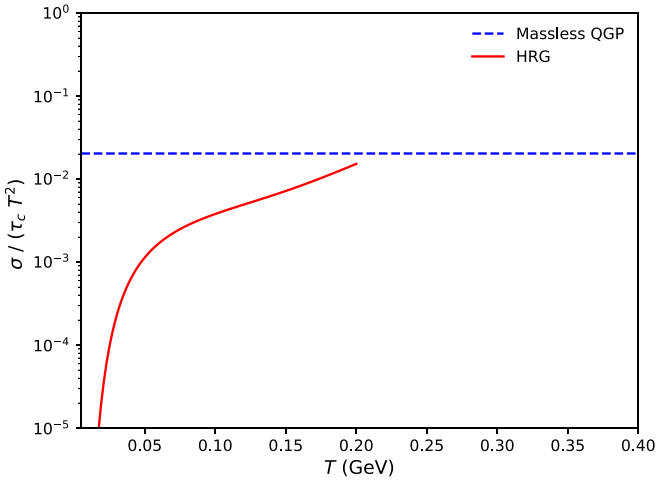

FIG. 1. Electrical conductivity σ normalized by $\tau_c T^2$ as a function of T for massless QGP and HRG.

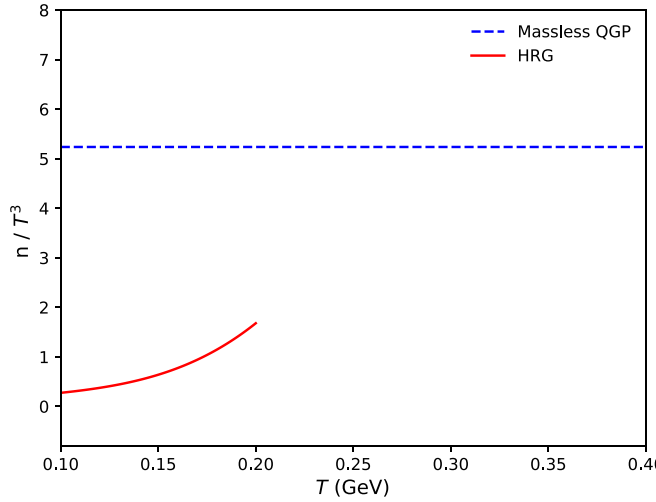

FIG. 2. Normalized number density $n/(T^3)$ vs T for massless QGP and HRG.

In Fig. 1, we have portrayed the normalized electrical conductivity $\sigma/\tau_c T^2$ with respect to temperature T. We take the help of Eq. (31) to get the expression of $\sigma_{\rm QGP}$ for massless QGP, which can be seen to be directly proportional to $\tau_c T^2$. Accordingly, we have obtained a horizontal line corresponding to $\sigma/\tau_c T^2 = 0.02$. For the hadronic temperature regime, we have presented the variation of scaled conductivity $\sigma/\tau_c T^2$ by resorting to the HRG model Eq. (24) at zero baryon chemical potential. For simplicity, we have assumed constant τ_c for all the hadrons to obtain the pattern of scaled $\sigma_{\rm HRG}$ in Fig. 1. The plot (red solid line) displays a sharp rise at low temperatures and eventually flattens as the temperature increases. The conductivity for the hadron gas obtained from the HRG model stays below the massless QGP (blue dashed line). The pattern is quite similar to the normalized thermodynamical quantities like pressure, energy density, etc., whose HRG estimations always remain below their massless QGP or Stefan-Boltzmann (SB) limits.

In Fig. 2, we have compared the numerical magnitudes of normalized number density $\frac{n}{T^3}$ for massless QGP (red solid line) and hadron gas (blue dashed line). We use Eq. (33) and Eq. (27) for massless QGP and hadron gas for the determination of the magnitude of $\frac{n}{T^3}$. For QGP, owing to the relation $n \propto T^3$, we get a horizontal line at $\frac{n}{T^3} \approx 5.23$. In contrast, in the hadron gas, our model calculation produces a monotonically increasing n or n/T^3 with respect to T. Again, we observe that, like conductivity, the number density value for hadron gas estimated from the HRG model stays below the massless QGP limit.

In Fig. 3, we have displayed the variation of the average velocity of different hadrons in the hadron gas with respect to their masses up to 2.6 GeV at two different temperatures: $T = 0.1$ GeV and $T = 0.2$ GeV. We have obtained the numerical values of $v_{\rm av}$ from Eq. (26) at zero baryonic chemical potential. The result shows a decrease in average velocity $v_{\rm av}$ of all the hadrons with respect to their masses. The lighter hadrons have high velocities compared to the heavier ones. An increase in temperature makes hadrons move with an increased velocity as the thermal energy increases with temperature. Moreover, we have also created a band to depict the range of velocity of all hadrons between $T = 0.1$ GeV and $T = 0.2$ GeV.

In Fig. 4, we have illustrated the change of relaxation or collision time of different hadrons with respect to their masses for two different temperature values: $T = 0.1$ GeV and $T = 0.2$ GeV. For the evaluation of collision time, we have relied on the expression of the hard-sphere scattering model of the collision set down in Eq. (25). For each T value, we take two different scattering lengths a to display the variation of τ_c with respect to both T and a. For a fixed a the relaxation time $\tau_c(T)$ decreases because of the increase of $v_{\rm av}(T)$ and $n(T)$ by following the Eq. (25). Similarly, for a given T, the relaxation time increases with a since $\tau_c \propto \frac{1}{a^2}$. Here we have chosen $a = 0.2$ fm and $a = 2$ fm, whose reason will be clear in Fig. 5.

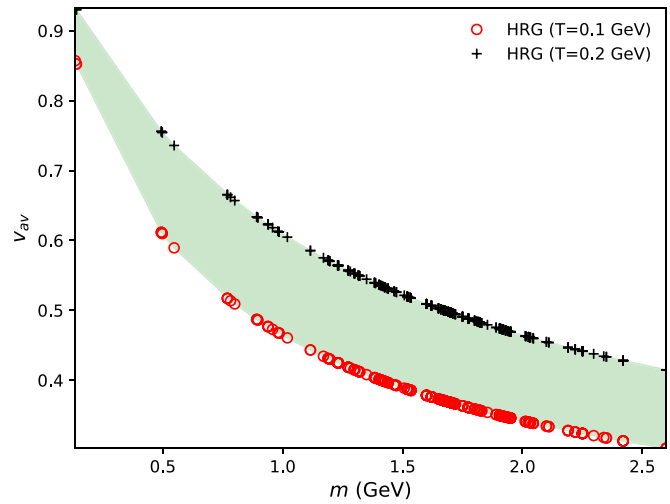

FIG. 3. Average velocity ($v_{\rm av}$) as a function of hadron mass (m) for all hadrons at two different temperatures: $T = 0.1$ GeV and $T = 0.2$ GeV.

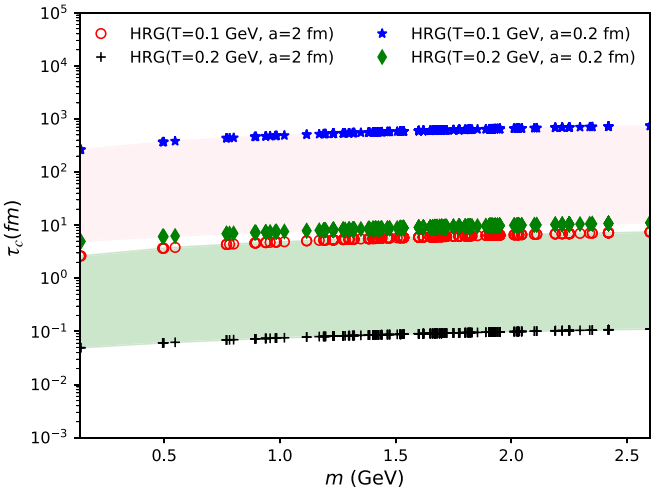

FIG. 4. Relaxation Time τ_c vs (m) for various hadrons at two different temperatures: $T = 0.1$ GeV and $T = 0.2$ GeV. Two different values of a (0.2 and 2 fm) are considered for each temperature.

Next, we have aimed to compile earlier estimated data of σ/T within the hadronic temperature domain, where few selective estimated results [127–129] are shown in Fig. 5. The order of magnitude for σ/T, obtained by Cassing *et al.* [127] (diamonds), Marty *et al.* [128] (stars), and Fraile *et al.* [129] (solid circles), are within the range 0.001 to 0.1. A long list of references [127–141] can be found for microscopic estimation of σ/T, whose order of magnitude will be located within 0.001 to 0.1 for hadronic temperature domain and 0.002 to 0.3 within quark temperature domain. Now, it can be seen that all the data obtained from earlier works within the hadronic temperature domain can be covered by altering a from 0.2 to 2 fm. For this reason, the same range of a has been considered in previous Fig. 4. We have also added a nonrelativistic version

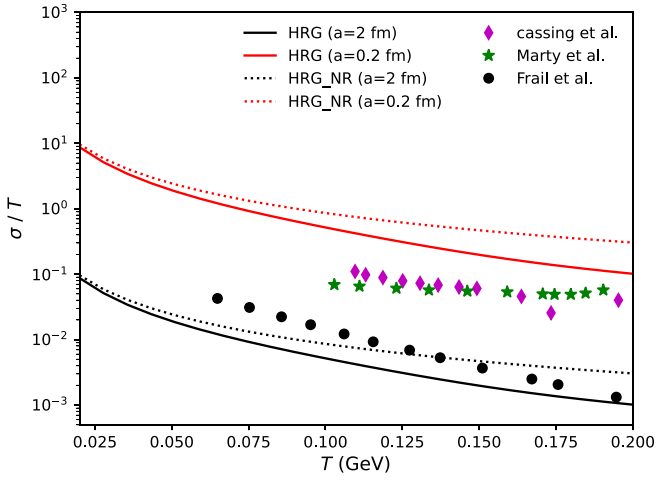

FIG. 5. Electrical conductivity σ/T vs T for HRG with temperature-dependent $\tau_c(T)$ at a = 0.2 and 2 fm and its comparison with the models of Cassing *et al.* [127], Marty *et al.* [128], Frail *et al.* [129]. Along with the relativistic estimations (solid lines), a nonrelativistic estimations (dotted lines) are also added to show the numerical contribution of relativistic correction.

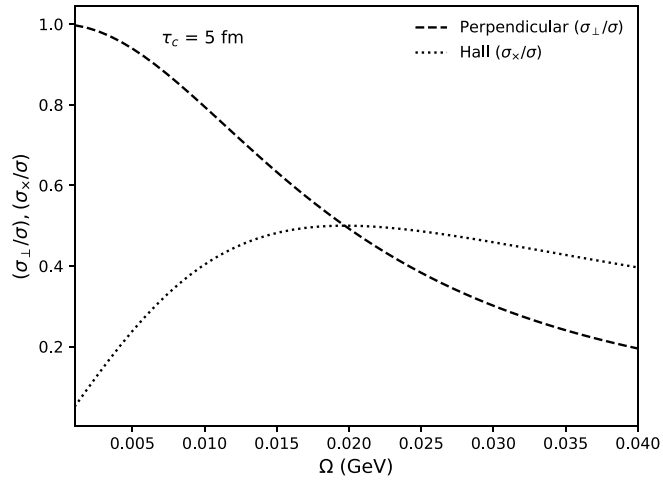

FIG. 6. Perpendicular and Hall electrical conductivity $\sigma_\perp/(\sigma)$, $\sigma_\times/(\sigma)$ vs Ω for HRG at $\tau_c = 5$ fm and $T = 0.150$ GeV.

of HRG estimations (dotted lines) along with our relativistic estimations (solid lines). Since the present framework may be considered as a relativistic extension of earlier Ref. [85], which was done in a nonrelativistic framework, so to see their difference, we have quickly gone through an HRG model in a nonrelativistic framework. Its quick formalism part is added in Appendix A 2.

To Fig. 5, we have gone through the estimations of σ/T in the absence of rotation. In presence of rotation the isotropic nature of σ/T converts into anistropic nature of σ/T, having multi components- $\sigma^{||}$, $\sigma^{\perp}$, and $\sigma^{\times}$. Interestingly, $\sigma^{||}$ in the presence of rotation is the same as σ, which is the isotropic conductivity in the absence of Ω. The expression of $\sigma(T)$ given in Eq. (24) has two components: thermodynamical phase space and relaxation time $\tau_c(T)$. The former component has a nontunable temperature profile, while the latter component can be tunable by tuning the magnitude of scattering cross section through a. We have used hard-sphere scattering cross-section relation for the expression of $\tau_c(T)$, given in Eq. (25). The temperature dependance of τ_c is mainly determined by $n(T)$ and $v_{\rm av}(T)$ which are displayed in the earlier Figs. 2 and 3. After calibrating our results without rotation with earlier estimations, we will now proceed to apply them to rotating hadronic matter.

In Fig. 6, we have depicted the variation of perpendicular and Hall conductivities $\sigma^{\perp,\times}$ normalized by the parallel conductivity $\sigma^{||} = \sigma$ as a function of Ω for a fixed $T = 0.150$ GeV. We have employed Eqs. (28), (29), and (24) for the numerical estimation of $\sigma^{\perp}$, $\sigma^{\times}$, and σ respectively for rotating HRG. In relation to Eq. (25) and Fig. 4, it is apparent that the relaxation time is a function of a, T, and m, i.e., $\tau_c = \tau_c(a, m, T)$. So, for a specific hadron in the system at a given temperature, it depends on the effective hard-sphere scattering length. In the beginning, let us consider a constant τ_c for estimating $\sigma^{||,\perp,\times}$ instead of the actual $\tau_c(a, m, T)$. By doing this, we can visualize only the thermodynamical phase space part of $\sigma^{||,\perp,\times}(T, \Omega)$. In this plot, we choose a value of $\tau_c = 5$ fm (25 GeV^{-1}), which falls in the band of τ_c obtained in Fig. 4 for $a = 2$ fm. In HICs, the average value of the local

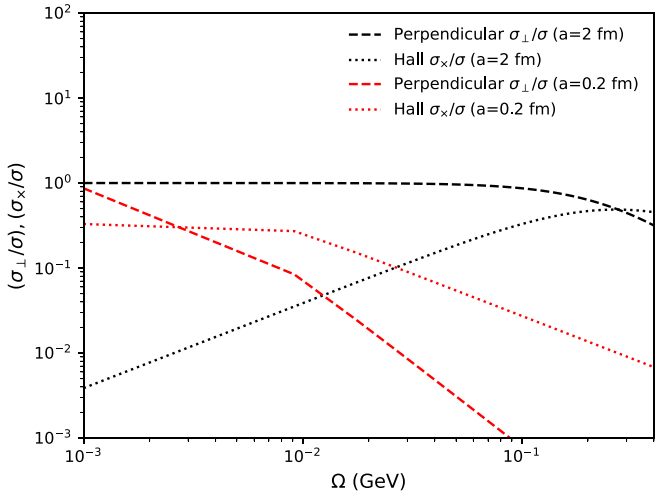

FIG. 7. Perpendicular and Hall electrical conductivity $(\sigma_\perp/\sigma, \sigma_\times/\sigma)$ vs Ω for HRG at $T = 0.150$ GeV.

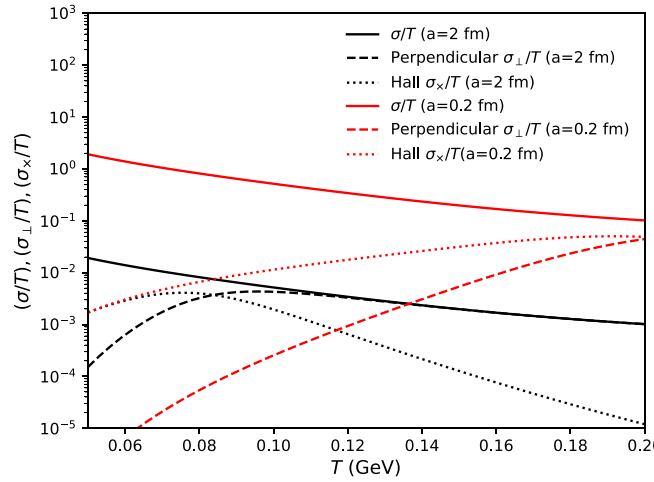

FIG. 8. Parallel, perpendicular, and Hall electrical conductivity $(\sigma/T, \sigma_\perp/T, \sigma_\times/T)$ as functions of temperature (T) for HRG with $\tau_c(T)$ and $\tau_\Omega = 6$ fm.

vorticity can be taken as a measure of the global vorticity or angular velocity of the system. The average vorticity for HIC has been calculated from various models [22,55,56,142]. Inspired by these studies, we choose the scale of the Ω axis from 0 to 0.04 GeV. $\sigma^\perp$ (or σ^0), the perpendicular conductivity of the rotating HRG corresponds to the current in the direction of the applied electric field in the XY plane. In the limit of $\Omega \to 0$, $\sigma^\perp$ reduces to conductivity σ. In our plot, this feature can be seen where $\frac{\sigma^\perp}{\sigma} \to 1$ as one approach to $\Omega \to 0$. Similarly, we can see the matrix in Eq. (23) that $\sigma^1 \equiv \sigma^\times$ drives the electric current in the XY plane of the rotating hadron gas; it drives current in the X direction if the electric field is in the Y direction and vice versa. In the limit $\Omega \to 0$, $\sigma^\times$ vanishes. The Hall conductivity $\sigma^\times$ shows interesting characteristics, it first increases with Ω to hit a peak where $\tau_\Omega \equiv \frac{1}{2\Omega}$ approaches τ_c and then decreases with further increase in Ω. From Fig. 6 one can notice that, for slowly rotating HRG, i.e., at low Ω, the $\sigma^\perp$ dominates over $\sigma^\times$ whereas, for a fastly rotating HRG, i.e., at high Ω we see that $\sigma^\perp < \sigma^\times$. Noticeably, the magnitude of $\sigma^{\perp,\times}/\sigma$ in the figure lies below one, i.e., $\sigma^{\perp,\times}/\sigma \leqslant 1$. This property can be understood by recognizing three different timescales associated with the rotating hadronic gas: $\tau_c \equiv \tau_c^{||}$, $\tau_c^\perp$, and $\tau_c^\times$. The effective relaxation times $\tau_c^\perp$ and $\tau_c^\times$ occurs in the mathematical expression of $\sigma^\perp$ and $\sigma^\times$ are given as follows:

$$\tau_c^\perp = \frac{\tau_c}{1 + \left(\frac{\tau_c}{\tau_\Omega}\right)^2}, \quad \tau_c^\times = \frac{\tau_c\left(\frac{\tau_c}{\tau_\Omega}\right)}{1 + \left(\frac{\tau_c}{\tau_\Omega}\right)^2}.$$

A glance at the above timescales suggests that $\tau_c^\perp < \tau_c$ and $\tau_c^\times < \tau_c$ which determines the ordering $\sigma^\perp < \sigma$ and $\sigma^\times < \sigma$.

We have delineated the variation of normalized conductivity $\frac{\sigma^{\perp,\times}}{\sigma}$ in relation to the angular velocity Ω of the hadronic medium at $T = 0.150$ GeV in Fig. 7. In contrast to Fig. 6, where we have interpreted the alternation of $\frac{\sigma^{\perp,\times}}{\sigma}$ graphically for a fixed value of $\tau_c = 5$ fm, we take here the individual τ_c of the rotating hadrons by using Eq. (25). For fixed $T = 0.150$ GeV and take two different values $a = (0.2\text{ fm}, 2\text{ fm})$ we have calculated $\tau_c = \tau_c(a, m, T)$ for different hadron resonances with mass m. The different values of a chosen here are the tuned scattering lengths obtained by the calibration done in Fig. 5. For the value of $a = 2$ fm, we see that for a rotating HRG with Ω in the range 0.001 to 0.02 GeV, the $\sigma^\perp$ is almost equal to σ and $\sigma^\times$ is negligible. This suggests an almost isotropic HRG with the scattering length $a = 2$ fm. Nevertheless, for $a = 0.2$ fm, we observe that in the range $\Omega = 0.01$–0.02 GeV there is a significant magnitude of $\sigma^\times$ which is around 10% to 15% of σ. Also, in the same range of Ω, one can notice a significant suppression of the $\sigma^\perp$ with respect to σ, which is around 90%. This suggests a highly anisotropic HRG with a hugely suppressed perpendicular conductivity $\sigma^\perp$ along with a large magnitude of Hall conductivity $\sigma^\times$. In Fig. 8, we have displayed the temperature dependence of the scaled conductivities σ/T for the rotating HRG at an angular speed $\Omega = 0.016$ GeV ($\tau_\Omega \approx 6$ fm). Similarly to the previous figure, we take two different values of $a\,(0.2\text{ fm}, 2\text{ fm})$ for the determination of $\tau_c(a, M, T)$ from Eq. (25). The plot represents a strong variation of both perpendicular $\sigma^\perp$ and Hall $\sigma^\times$ conductivities in relation to temperature T. For a rotating HRG with $a = 2$ fm, the $\sigma^\perp$ almost merges with σ for temperature $T \geqslant 0.12$ GeV. This implies an almost isotropic rotating HRG with $\sigma^\perp \approx \sigma$. Nevertheless, one can define a region of temperature $T = 0.05$–0.14 GeV where the system still has a significant magnitude of $\sigma^\times$ with $\sigma/\sigma^\times \sim 10$ or less. On the other hand, in a rotating HRG with $a = 0.2$ fm, there is a remarkable suppression of $\sigma^\perp$ with respect to σ in the T range 0.10–0.20 GeV. The magnitude of the suppression is around 90% at $T = 0.12$ GeV. These observations suggest strongly anisotropic rotating HRG with $a = 0.2$ fm. There is also a significant magnitude of Hall conductivity $\sigma^\times$ for T more than 0.14 GeV, i.e., $\sigma/\sigma^\times \leqslant 10$ for $T \geqslant 0.14$ GeV.

In the end, we can find a succinct qualitative message from our detailed quantitative investigations. It says that Coriolis force can have a noticeable impact on creating an anisotropic conductivity tensor at a finite rotation of the HRG system, as done by the Lorentz force at a finite magnetic field.

However, this noticeable impact will quantitatively depend on the hadronic scattering strengths, quantified by a in our study. We have shown the noticeable and non-noticeable impact for $a = 0.2$ fm and $a = 2$ fm, respectively. Another debatable point is that how fast or slow the angular velocity will decay with time [22,55,56] so that hadronic matter will face it. In this context, a possibility of noticeable impact for any values within the range $\Omega = 0.001$–0.02 GeV can be found.

IV. SUMMARY

In this work, we have made an effort to visualize the effect of Coriolis force on electrical conductivity in the hadron resonance gas model. The coefficient of proportionality between electrical current density and electrical field is known as electrical conductivity. Using the Boltzmann transport equation and the relaxation time approximation, we have calculated their microscopic expressions within the framework of kinetic theory based on their macroscopic formulations. The Coriolis force in rotating frames leads to similar anisotropy in the electrical conductivity tensor (σ) as the Lorentz force introduced in the presence of a magnetic field. The generated anisotropy is categorized into three parts: the Hall, perpendicular, and parallel components. The parallel component of electrical conductivity remains unaffected as it is independent of the relaxation time of the medium. However, we observe the variations in the scaled electrical conductivity of the perpendicular and Hall components with temperature in the presence of Coriolis force. In the absence of rotation, the scaled electrical conductivity (scaled with $\tau_c T^2$) increases with temperature but stays below the results obtained for massless QGP or SB limits similar to the normalized thermodynamical quantities like pressure, energy density, etc. The average velocity of particles decreases monotonically with mass, which leads to an increase in particle relaxation time as a function of their respective masses. We estimate the relaxation time using the hard-sphere scattering model. We observed that the earlier estimations of (σ/T) could be tuned by varying the scattering lengths a from 0.2 to 2 fm. A monotonic decreasing trend is observed in electrical conductivity with temperature in the absence of rotation. The presence of the Coriolis force induces an anisotropic nature in electrical conductivity. We observed that as the angular velocity (Ω) of the rotating hadron gas system increases, the perpendicular component of electrical conductivity decreases. As the rotation speed (Ω) approaches zero, the perpendicular component converges to the overall conductivity σ. On the contrary, the Hall component vanishes towards small Ω. The Hall component shows interesting behavior; initially, it increases with Ω, reaching a peak when the characteristic rotation time (τ_Ω) becomes comparable to the relaxation time τ_c and then decreases with further increase in Ω. Therefore, we can conclude that in a slowly rotating HRG, with low Ω, $\sigma^\perp$ dominates over the Hall conductivity $\sigma^\times$, whereas for a fastly rotating (large Ω) HRG $\sigma^\times > \sigma^\perp$. Even more interestingly, we observe that this flip from $\sigma^\perp$ dominance to $\sigma^\times$ dominance occurs at relatively smaller angular velocities for systems with smaller scattering lengths. In the end, we estimate the variation of electrical conductivity components with temperature at a fixed angular speed. We observed a strong variation in both perpendicular and Hall components with temperature. With the chosen angular speed $\Omega = 0.016$ GeV ($\tau_\Omega \approx 6$ fm) the $\sigma^\perp$ almost merges with σ above for temperature $T \approx 0.12$ GeV for $a = 2$ fm. This implies an almost isotropic rotating HRG with $\sigma^\perp \approx \sigma$. On the other hand, for $a = 0.2$ fm, suppression of $\sigma^\perp$ with respect to σ is notably strong up to $T \approx 0.20$ GeV, which suggests strongly anisotropic rotating HRG with $a = 0.2$ fm.

ACKNOWLEDGMENTS

N.P. and A.D. gratefully acknowledge the Ministry of Education (MoE), Government of India. The authors extend their thanks to Snigdha Ghosh for sharing valuable materials and insights on HRG model calculations.

APPENDIX: CONDUCTIVITY IN RELATIVISTIC AND NON-RELATIVISTIC HADRON GAS USING BOLTZMANN TRANSPORT EQUATION

1. Calculation of current density

The current density J_i can be readily calculated from Eq. (1) after the determination of δf. To calculate δf let us substitute the ansatz $\delta f = -\vec{p}\cdot\vec{X}(\frac{\partial f^0}{\partial E})$ in the Eq. (21),

$$\frac{\partial f^0}{\partial E}\frac{\vec{p}}{p_0}\cdot(q\vec{\tilde{E}}) + 2\vec{p}\cdot\left[\vec{\Omega}\times\frac{\partial\delta f}{\partial\vec{p}}\right] = \frac{-\delta f}{\tau_c}$$

$$\Rightarrow \frac{\partial f^0}{\partial E}\frac{\vec{p}}{E}\cdot(q\vec{\tilde{E}}) + 2\vec{p}\cdot\left[\vec{\Omega}\times\frac{\partial(-\vec{p}\cdot\vec{X}\frac{\partial f^0}{\partial E})}{\partial\vec{p}}\right] = \frac{\vec{p}\cdot\vec{X}}{\tau_c}\frac{\partial f^0}{\partial E},$$

which, after simplification, becomes

$$\left[\frac{q\vec{\tilde{E}}}{E} + 2(\vec{X}\times\vec{\Omega})\right]\cdot\vec{p}\frac{\partial f^0}{\partial E} = \frac{\vec{X}}{\tau_c}\cdot\left(\vec{p}\frac{\partial f^0}{\partial E}\right), \tag{A1}$$

since $\vec{p}$ is arbitrary in Eq. (A1), the following relation is valid for $\vec{X}$,

$$\left[\frac{q\vec{\tilde{E}}}{E} + 2(\vec{X}\times\vec{\Omega})\right] = \frac{\vec{X}}{\tau_c}. \tag{A2}$$

Substituting the result, $\vec{X}\times\vec{\Omega} = -\gamma\Omega\hat{e} + \gamma\Omega(\hat{\omega}\cdot\hat{e})\hat{\omega} + \alpha\Omega(\hat{e}\times\hat{\omega})$, in Eq. (A2), we have

$$\left(\frac{q\vec{\tilde{E}}}{E} - 2\Omega\gamma\right)\hat{e} + 2\gamma\Omega(\hat{\omega}\cdot\hat{e})\hat{\omega} + 2\alpha\Omega(\hat{e}\times\hat{\omega}) = \frac{\alpha}{\tau_c}\hat{e} + \frac{\beta}{\tau_c}\hat{\omega} + \frac{\gamma}{\tau_c}(\hat{e}\times\hat{\omega}). \tag{A3}$$

By equating the coefficients of the linearly independent basis vectors in Eq. (A3), we get

$$\frac{q\tilde{E}}{E} - \frac{\gamma}{\tau_\Omega} = \frac{\alpha}{\tau_c}, \quad \frac{\gamma}{\tau_\Omega}(\hat{\omega}\cdot\hat{e}) = \frac{\beta}{\tau_c}, \quad \frac{\alpha}{\tau_\Omega} = \frac{\gamma}{\tau_c},$$

where $\tau_\Omega \equiv \frac{1}{2\Omega}$. Simplifying the above three equations, we get the following values for α, β, and γ:

$$\alpha = \frac{\tau_c\left(\frac{q\tilde{E}}{E}\right)}{1+\left(\frac{\tau_c}{\tau_\Omega}\right)^2}, \quad \gamma = \frac{\tau_c\left(\frac{\tau_c}{\tau_\Omega}\right)\left(\frac{q\tilde{E}}{E}\right)}{1+\left(\frac{\tau_c}{\tau_\Omega}\right)^2}, \quad \beta = \frac{\tau_c\left(\frac{\tau_c}{\tau_\Omega}\right)^2(\hat{\omega}\cdot\hat{e})\left(\frac{q\tilde{E}}{E}\right)}{1+\left(\frac{\tau_c}{\tau_\Omega}\right)^2}.$$

By substituting the expressions of α, β, and γ, we get the explicit form of the δf as

$$\begin{aligned}
\delta f &= -\vec{p}\cdot\vec{X}\frac{\partial f^0}{\partial E} = -\frac{\partial f^0}{\partial E}\vec{p}\cdot(\alpha\hat{e}+\beta\hat{\omega}+\gamma(\hat{e}\times\hat{\omega})) \\
&= -\frac{1}{E}\frac{\partial f^0}{\partial E}\left[\frac{q\tau_c\tilde{E}}{1+\left(\frac{\tau_c}{\tau_\Omega}\right)^2}\hat{e}\cdot\vec{p}+\frac{\tau_c\left(\frac{\tau_c}{\tau_\Omega}\right)^2(\hat{\omega}\cdot\hat{e})q\tilde{E}}{1+\left(\frac{\tau_c}{\tau_\Omega}\right)^2}\hat{\omega}\cdot\vec{p}+\frac{\tau_c\left(\frac{\tau_c}{\tau_\Omega}\right)q\tilde{E}}{1+\left(\frac{\tau_c}{\tau_\Omega}\right)^2}(\hat{e}\times\hat{\omega})\cdot\vec{p}\right] \\
&= -\frac{1}{E}\frac{\partial f^0}{\partial E}\left(\frac{q\tau_c}{1+\left(\frac{\tau_c}{\tau_\Omega}\right)^2}\right)\left[\vec{\tilde{E}}\cdot\vec{p}+\left(\frac{\tau_c}{\tau_\Omega}\right)^2(\hat{\omega}\cdot\vec{\tilde{E}})(\hat{\omega}\cdot\vec{p})+\left(\frac{\tau_c}{\tau_\Omega}\right)(\vec{\tilde{E}}\times\hat{\omega})\cdot\vec{p}\right] \\
&= -\frac{1}{E}\frac{\partial f^0}{\partial E}\left(\frac{q\tau_c}{1+\left(\frac{\tau_c}{\tau_\Omega}\right)^2}\right)\left[\tilde{E}_j p^j+\left(\frac{\tau_c}{\tau_\Omega}\right)^2\omega_j\tilde{E}_j\omega_q p^q+\left(\frac{\tau_c}{\tau_\Omega}\right)\epsilon_{qjk}\tilde{E}_j\omega_k p^q\right] \\
&= -\frac{q}{E}\frac{\partial f^0}{\partial E}\left(\frac{\tau_c}{1+\left(\frac{\tau_c}{\tau_\Omega}\right)^2}\right)\left[\delta_{jq}+\left(\frac{\tau_c}{\tau_\Omega}\right)^2\omega_j\omega_q+\left(\frac{\tau_c}{\tau_\Omega}\right)\epsilon_{qjk}\omega_k\right]\tilde{E}_j p^q. \qquad \text{(A4)}
\end{aligned}$$

The δf obtained in Eq. (A4) solves Eq. (21). Now, we will retain the label r and write the current density for the hadronic species r as

$$J_r^i = -g_r q_r^2\int\frac{d^3\vec{p}}{(2\pi)^3}\frac{p^i p^l}{E^2}\frac{\partial f_r^0}{\partial E}\left(\frac{\tau_c}{1+\left(\frac{\tau_c}{\tau_\Omega}\right)^2}\right)\left[\delta_{jl}+\left(\frac{\tau_c}{\tau_\Omega}\right)^2\omega_j\omega_l+\left(\frac{\tau_c}{\tau_\Omega}\right)\epsilon_{ljk}\omega_k\right]\tilde{E}_j. \qquad \text{(A5)}$$

We can substitute the angular average, $\int d^3\vec{p}\,p^i p^l = \int d^3p(\frac{p^2}{3})\delta_{il}$, $(4\pi p^2 dp \equiv d^3p)$ and the static limit ($\vec{u}=0$) identity, $\frac{\partial f_r^0}{\partial E} = -\frac{f_r^0(1+\xi f_r^0)}{T}$ in Eq. (A5) to get

$$J_r^i = \frac{g_r q_r^2}{3T}\int\frac{d^3\vec{p}}{(2\pi)^3}\frac{p^2}{E^2}\left(\frac{\tau_c}{1+\left(\frac{\tau_c}{\tau_\Omega}\right)^2}\right)\left[\delta_{ij}+\left(\frac{\tau_c}{\tau_\Omega}\right)\epsilon_{ijk}\omega_k+\left(\frac{\tau_c}{\tau_\Omega}\right)^2\omega_i\omega_j\right]\tilde{E}_j f_r^0\left(1+\xi f_r^0\right). \qquad \text{(A6)}$$

Comparing the macroscopic expression (Ohm's law) $J_r^i = \sigma_r^{ij}\tilde{E}_j$ with the Eq. (A6) we get

$$\begin{aligned}
\sigma_r^{ij} &= \frac{g_r q_r^2}{3T}\int\frac{d^3\vec{p}}{(2\pi)^3}\frac{p^2}{E^2}\left(\frac{\tau_c}{1+\left(\frac{\tau_c}{\tau_\Omega}\right)^2}\right)\left[\delta_{ij}+\left(\frac{\tau_c}{\tau_\Omega}\right)\epsilon_{ijk}\omega_k+\left(\frac{\tau_c}{\tau_\Omega}\right)^2\omega_i\omega_j\right]f_r^0\left(1+\xi f_r^0\right) \\
\Rightarrow\ \sigma_r^{ij} &= \sigma_r^0\delta_{ij}+\sigma_r^1\epsilon_{ijk}\omega_k+\sigma_r^2\omega_i\omega_j,
\end{aligned}$$

where we have

$$\sigma_r^n = \frac{g_r q_r^2}{3T}\int\frac{d^3p}{(2\pi)^3}\frac{\tau_c\left(\frac{\tau_c}{\tau_\Omega}\right)^n}{1+\left(\frac{\tau_c}{\tau_\Omega}\right)^2}\times\frac{p^2}{E^2}f_r^0\left(1+\xi f_r^0\right), \qquad \text{(A7)}$$

where σ_r^0, σ_r^1, and σ_r^2 are scalars that make up the conductivity tensor. The total conductivity tensor is given by, $\sigma^{ij} = \sum_r \sigma_r^{ij}$. The explicit form of total conductivity tensor and scalar conductivity are

$$\begin{aligned}
\sigma^{ij} &= \sum_r\frac{g_r q_r^2}{3T}\int\frac{d^3\vec{p}}{(2\pi)^3}\frac{p^2}{E^2}\left(\frac{\tau_c}{1+\left(\frac{\tau_c}{\tau_\Omega}\right)^2}\right)\left[\delta_{ij}+\left(\frac{\tau_c}{\tau_\Omega}\right)\epsilon_{ijk}\omega_k+\left(\frac{\tau_c}{\tau_\Omega}\right)^2\omega_i\omega_j\right]f_r^0\left(1+\xi f_r^0\right) \\
\sigma^n &= \sum_r\frac{g_r q_r^2}{3T}\int\frac{d^3p}{(2\pi)^3}\frac{\tau_c\left(\frac{\tau_c}{\tau_\Omega}\right)^n}{1+\left(\frac{\tau_c}{\tau_\Omega}\right)^2}\times\frac{p^2}{E^2}f_r^0\left(1+\xi f_r^0\right). \qquad \text{(A8)}
\end{aligned}$$

The total current density in the rotating HRG can also be written as

$$\vec{J} = \sigma^0 \vec{\tilde{E}} + \sigma^1(\vec{\tilde{E}} \times \hat{\omega}) + \sigma^2(\hat{\omega} \cdot \vec{\tilde{E}})\hat{\omega}. \tag{A9}$$

2. Formulas for nonrelativistic HRG

Since, present work is relativistic extension of earlier Ref. [85], which was done in nonrelativistic framework, so to see their difference, we have quickly gone through a HRG model in nonrelativistic framework. One can rewrite Eq. (22) in nonrelativistic HRG framework as

$$\sigma^n = \frac{gq^2}{T}\int \frac{d^3p}{(2\pi)^3}\frac{\tau_c\left(\frac{\tau_c}{\tau_\Omega}\right)^n}{1+\left(\frac{\tau_c}{\tau_\Omega}\right)^2} \times \frac{v^2}{3} f^0(1-f^0), (\vec{v} = \vec{p}/m, \text{ and } E = p^2/2m)$$

$$\Rightarrow \sigma^n = \frac{gq^2}{3T}\int \frac{d^3p}{(2\pi)^3}\frac{\tau_c\left(\frac{\tau_c}{\tau_\Omega}\right)^n}{1+\left(\frac{\tau_c}{\tau_\Omega}\right)^2} \times \frac{p^2}{m^2} f^0(1-f^0). \tag{A10}$$

Equation (A10) is useful for calculating conductivity for a single-component nonrelativistic fluid. The nonrelativistic HRG expression can be obtained from Eq. (A10) as

$$\sigma^n = \sum_r \frac{g_r q_r^2}{3T}\int \frac{d^3p}{(2\pi)^3}\frac{\tau_c\left(\frac{\tau_c}{\tau_\Omega}\right)^n}{1+\left(\frac{\tau_c}{\tau_\Omega}\right)^2} \times \frac{p^2}{m_r^2} f_r^0\left(1+\xi f_r^0\right). \tag{A11}$$

The formulas for parallel, perpendicular, and Hall conductivity for nonrelativistic HRG are given by

$$\sigma^{\parallel}_{\text{NHRG}} \equiv \sigma_{\text{NHRG}} = \sum_B \frac{g_B q_B^2}{3T}\int \frac{d^3p}{(2\pi)^3}\tau_c \times \frac{p^2}{m_B^2} f^0(1-f^0) + \sum_M \frac{g_M q_M^2}{3T}\int \frac{d^3p}{(2\pi)^3}\tau_c \times \frac{p^2}{m_M^2} f^0(1+f^0), \tag{A12}$$

$$\sigma^{\perp}_{\text{NHRG}} = \sum_B \frac{g_B q_B^2}{3T}\int \frac{d^3p}{(2\pi)^3}\frac{\tau_c}{1+\left(\frac{\tau_c}{\tau_\Omega}\right)^2} \times \frac{p^2}{m_B^2} f^0(1-f^0) + \sum_M \frac{g_M q_M^2}{3T}\int \frac{d^3p}{(2\pi)^3}\frac{\tau_c}{1+\left(\frac{\tau_c}{\tau_\Omega}\right)^2} \times \frac{p^2}{m_M^2} f^0(1+f^0), \tag{A13}$$

$$\sigma^{\times}_{\text{NHRG}} = \sum_B \frac{g_B q_B^2}{3T}\int \frac{d^3p}{(2\pi)^3}\frac{\tau_c\left(\frac{\tau_c}{\tau_\Omega}\right)}{1+\left(\frac{\tau_c}{\tau_\Omega}\right)^2} \times \frac{p^2}{m_B^2} f^0(1-f^0) + \sum_M \frac{g_M q_M^2}{3T}\int \frac{d^3p}{(2\pi)^3}\frac{\tau_c\left(\frac{\tau_c}{\tau_\Omega}\right)}{1+\left(\frac{\tau_c}{\tau_\Omega}\right)^2} \times \frac{p^2}{m_M^2} f^0(1+f^0). \tag{A14}$$

The relaxation time of any nonrelativistic hadron can be written as

$$\tau_c = 1/\left(n_{\text{NHRG}} v_{\text{av}}^{\text{NH}} \pi a^2\right), \tag{A15}$$

where hard-sphere cross section πa^2 is considered for hadron, having average velocity

$$v_{\text{av}}^{\text{NH}} = \int \frac{d^3p}{(2\pi)^3}\frac{p}{m} f_0 \Big/ \int \frac{d^3p}{(2\pi)^3} f_0. \tag{A16}$$

Each hadron will face the entire density of the system

$$n_{\text{NHRG}} = \sum_B g_B \int_0^\infty \frac{d^3p}{(2\pi)^3}\frac{1}{e^{E/T}+1} + \sum_M g_M \int_0^\infty \frac{d^3p}{(2\pi)^3}\frac{1}{e^{E/T}-1}, (E = p^2/2m), \tag{A17}$$

where g_B and g_M are baryon and meson spin degeneracy factors, respectively.

[1] L. Adamczyk *et al.* (STAR Collaboration), Global Λ hyperon polarization in nuclear collisions: evidence for the most vortical fluid, Nature (London) **548**, 62 (2017).

[2] Z.-T. Liang and X.-N. Wang, Globally polarized quark-gluon plasma in non-central *A*+*A* collisions, Phys. Rev. Lett. **94**, 102301 (2005); **96**, 039901(E) (2006).

[3] F. Becattini, F. Piccinini, and J. Rizzo, Angular momentum conservation in heavy-ion collisions at very high energy, Phys. Rev. C **77**, 024906 (2008).

[4] J. Adam *et al.* (STAR Collaboration), Global polarization of Λ hyperons in Au+Au collisions at $\sqrt{s_{NN}} = 200$ GeV, Phys. Rev. C **98**, 014910 (2018).

[5] S. Acharya *et al.* (ALICE Collaboration), Evidence of spin-orbital angular momentum interactions in relativistic heavy-ion collisions, Phys. Rev. Lett. **125**, 012301 (2020).

[6] M. S. Abdallah *et al.* (STAR Collaboration), Pattern of global spin alignment of ϕ and K^{*0} mesons in heavy-ion collisions, Nature (London) **614**, 244 (2023).

[7] S. Acharya *et al.* (ALICE Collaboration), Measurement of the J/ψ polarization with respect to the event plane in Pb-Pb collisions at the LHC, Phys. Rev. Lett. **131**, 042303 (2023).

[8] F. Becattini and F. Piccinini, The ideal relativistic spinning gas: Polarization and spectra, Ann. Phys. **323**, 2452 (2008).

[9] F. Becattini, V. Chandra, L. Del Zanna, and E. Grossi, Relativistic distribution function for particles with spin at local thermodynamical equilibrium, Ann. Phys. **338**, 32 (2013).

[10] F. Becattini, L. P. Csernai, and D. J. Wang, Λ polarization in peripheral heavy-ion collisions, Phys. Rev. C **88**, 034905 (2013; F. Becattini, L. P. Csernai, D. J. Wang, and Y. L. Xie, *ibid.* **93**, 069901(E) (2016).

[11] B. Betz, M. Gyulassy, and G. Torrieri, Polarization probes of vorticity in heavy-ion collisions, Phys. Rev. C **76**, 044901 (2007).

[12] Z.-T. Liang and X.-N. Wang, Spin alignment of vector mesons in non-central a+a collisions, Phys. Lett. B **629**, 20 (2005).

[13] J.-H. Gao, S.-W. Chen, W.-T. Deng, Z.-T. Liang, Q. Wang, and X.-N. Wang, Global quark polarization in noncentral $a + a$ collisions, Phys. Rev. C **77**, 044902 (2008).

[14] X.-G. Huang, P. Huovinen, and X.-N. Wang, Quark polarization in a viscous quark-gluon plasma, Phys. Rev. C **84**, 054910 (2011).

[15] F. Becattini, M. Buzzegoli, and A. Palermo, Spin-thermal shear coupling in a relativistic fluid, Phys. Lett. B **820**, 136519 (2021).

[16] X.-L. Xia, H. Li, Z.-B. Tang, and Q. Wang, Probing vorticity structure in heavy-ion collisions by local Λ polarization, Phys. Rev. C **98**, 024905 (2018).

[17] W. Florkowski, B. Friman, A. Jaiswal, and E. Speranza, Relativistic fluid dynamics with spin, Phys. Rev. C **97**, 041901(R) (2018).

[18] W. Florkowski, B. Friman, A. Jaiswal, R. Ryblewski, and E. Speranza, Spin-dependent distribution functions for relativistic hydrodynamics of spin-$\frac{1}{2}$ particles, Phys. Rev. D **97**, 116017 (2018).

[19] W. Florkowski, A. Kumar, R. Ryblewski, and R. Singh, Spin polarization evolution in a boost-invariant hydrodynamical background, Phys. Rev. C **99**, 044910 (2019).

[20] D.-X. Wei, W.-T. Deng, and X.-G. Huang, Thermal vorticity and spin polarization in heavy-ion collisions, Phys. Rev. C **99**, 014905 (2019).

[21] H.-Z. Wu, L.-G. Pang, X.-G. Huang, and Q. Wang, Local spin polarization in 200 GeV Au+Au and 2.76 TeV Pb+Pb collisions, Nucl. Phys. A **1005**, 121831 (2021).

[22] X.-G. Huang, J. Liao, Q. Wang, and X.-L. Xia, Vorticity and spin polarization in heavy ion collisions: Transport models, Lect. Notes Phys. **987**, 281 (2021).

[23] B. Fu, S. Y. F. Liu, L. Pang, H. Song, and Y. Yin, Shear-induced spin polarization in heavy-ion collisions, Phys. Rev. Lett. **127**, 142301 (2021).

[24] X.-G. Deng, X.-G. Huang, and Y.-G. Ma, Lambda polarization in ^{108}Ag $+^{108}$Ag and ^{197}Au $+^{197}$Au collisions around a few gev, Phys. Lett. B **835**, 137560 (2022).

[25] H. Li, X.-L. Xia, X.-G. Huang, and H. Z. Huang, Global spin polarization of multistrange hyperons and feed-down effect in heavy-ion collisions, Phys. Lett. B **827**, 136971 (2022).

[26] J.-H. Gao, Z.-T. Liang, S. Pu, Q. Wang, and X.-N. Wang, Chiral anomaly and local polarization effect from the quantum kinetic approach, Phys. Rev. Lett. **109**, 232301 (2012).

[27] J.-W. Chen, S. Pu, Q. Wang, and X.-N. Wang, Berry curvature and four-dimensional monopoles in the relativistic chiral kinetic equation, Phys. Rev. Lett. **110**, 262301 (2013).

[28] R. H. Fang, L. G. Pang, Q. Wang, and X. N. Wang, Polarization of massive fermions in a vortical fluid, Phys. Rev. C **94**, 024904 (2016).

[29] R. H. Fang, J. Y. Pang, Q. Wang, and X. N. Wang, Pseudoscalar condensation induced by chiral anomaly and vorticity for massive fermions, Phys. Rev. D **95**, 014032 (2017).

[30] J.-hua Gao and Q. Wang, Magnetic moment, vorticity-spin coupling and parity-odd conductivity of chiral fermions in 4-dimensional Wigner functions, Phys. Lett. B **749**, 542 (2015).

[31] Y. Hidaka, S. Pu, and D.-L. Yang, Relativistic chiral kinetic theory from quantum field theories, Phys. Rev. D **95**, 091901(R) (2017).

[32] J.-H. Gao, S. Pu, and Q. Wang, Covariant chiral kinetic equation in the Wigner function approach, Phys. Rev. D **96**, 016002 (2017).

[33] J.-H. Gao, Z.-T. Liang, Q. Wang, and X.-N. Wang, Disentangling covariant Wigner functions for chiral fermions, Phys. Rev. D **98**, 036019 (2018).

[34] A. Huang, S. Shi, Y. Jiang, J. Liao, and P. Zhuang, Complete and consistent chiral transport from Wigner function formalism, Phys. Rev. D **98**, 036010 (2018).

[35] J.-H. Gao, J.-Y. Pang, and Q. Wang, Chiral vortical effect in Wigner function approach, Phys. Rev. D **100**, 016008 (2019).

[36] J.-H. Gao and Z.-T. Liang, Relativistic quantum kinetic theory for massive fermions and spin effects, Phys. Rev. D **100**, 056021 (2019).

[37] K. Hattori, Y. Hidaka, and D.-L. Yang, Axial kinetic theory and spin transport for fermions with arbitrary mass, Phys. Rev. D **100**, 096011 (2019).

[38] Z. Wang, X. Guo, S. Shi, and P. Zhuang, Mass correction to chiral kinetic equations, Phys. Rev. D **100**, 014015 (2019).

[39] N. Weickgenannt, X. L. Sheng, E. Speranza, Q. Wang, and D. H. Rischke, Kinetic theory for massive spin-1/2 particles from the Wigner-function formalism, Phys. Rev. D **100**, 056018 (2019).

[40] D.-L. Yang, K. Hattori, and Y. Hidaka, Effective quantum kinetic theory for spin transport of fermions with collsional effects, J. High Energy Phys. 07 (2020) 070.

[41] N. Weickgenannt, E. Speranza, X. L. Sheng, Q. Wang, and D. H. Rischke, Generating spin polarization from vorticity through nonlocal collisions, Phys. Rev. Lett. **127**, 052301 (2021).

[42] N. Weickgenannt, E. Speranza, X. L. Sheng, Q. Wang, and D. H. Rischke, Derivation of the nonlocal collision term in the relativistic Boltzmann equation for massive spin-1/2 particles from quantum field theory, Phys. Rev. D **104**, 016022 (2021).

[43] F. Becattini and L. Ferroni, The microcanonical ensemble of the ideal relativistic quantum gas with angular momentum conservation, Eur. Phys. J. C **52**, 597 (2007).

[44] F. Becattini and L. Tinti, The ideal relativistic rotating gas as a perfect fluid with spin, Ann. Phys. **325**, 1566 (2010).

[45] F. Becattini, G. Inghirami, V. Rolando, A. Beraudo, L. Del Zanna, A. De Pace, M. Nardi, G. Pagliara, and V. Chandra, A study of vorticity formation in high energy nuclear collisions, Eur. Phys. J. C **75**, 406 (2015); **78**, 354 (2018).

[46] S.-w. Chen, J. Deng, J.-h. Gao, and Q. Wang, A general derivation of differential cross section in quark-quark and quark-gluon scatterings at fixed impact parameter, Front. Phys. China **4**, 509 (2009).

[47] F. Becattini, Hydrodynamics of fluids with spin, Phys. Part. Nucl. Lett. **8**, 801 (2011).

[48] W. Florkowski, A. Kumar, and R. Ryblewski, Relativistic hydrodynamics for spin-polarized fluids, Prog. Part. Nucl. Phys. **108**, 103709 (2019).

[49] W. Florkowski, A. Kumar, and R. Ryblewski, Thermodynamic versus kinetic approach to polarization-vorticity coupling, Phys. Rev. C **98**, 044906 (2018).
[50] F. Becattini, W. Florkowski, and E. Speranza, Spin tensor and its role in non-equilibrium thermodynamics, Phys. Lett. B **789**, 419 (2019).
[51] S. Bhadury, W. Florkowski, A. Jaiswal, A. Kumar, and R. Ryblewski, Relativistic dissipative spin dynamics in the relaxation time approximation, Phys. Lett. B **814**, 136096 (2021).
[52] S. Bhadury, W. Florkowski, A. Jaiswal, A. Kumar, and R. Ryblewski, Dissipative spin dynamics in relativistic matter, Phys. Rev. D **103**, 014030 (2021).
[53] A. Daher, A. Das, W. Florkowski, and R. Ryblewski, Equivalence ofcanonical and phenomenological formulations of spin hydrodynamics, Phys. Rev. C **108**, 024902 (2023).
[54] S. Bhadury, W. Florkowski, A. Jaiswal, A. Kumar, and R. Ryblewski, Relativistic spin magnetohydrodynamics, Phys. Rev. Lett. **129**, 192301 (2022).
[55] W.-T. Deng and X.-G. Huang, Vorticity in heavy-ion collisions, Phys. Rev. C **93**, 064907 (2016).
[56] Y. Jiang, Z.-W. Lin, and J. Liao, Rotating quark-gluon plasma in relativistic heavy-ion collisions, Phys. Rev. C **94**, 044910 (2016).
[57] L.-G. Pang, H. Petersen, Q. Wang, and X.-N. Wang, Vortical fluid and Λ spin correlations in high-energy heavy-ion collisions, Phys. Rev. Lett. **117**, 192301 (2016).
[58] H. Li, L.-G. Pang, Q. Wang, and X.-L. Xia, Global Λ polarization in heavy-ion collisions from a transport model, Phys. Rev. C **96**, 054908 (2017).
[59] X.-G. Huang, Vorticity and spin polarization—A theoretical perspective, Nucl. Phys. A **1005**, 121752 (2021).
[60] K. K. Pradhan, B. Sahoo, D. Sahu, and R. Sahoo, Thermodynamics of a rotating hadron resonance gas with van der Waals interaction, arXiv:2304.05190 [hep-ph].
[61] B. Sahoo, C. R. Singh, D. Sahu, R. Sahoo, and J.-e. Alam, Impact of vorticity and viscosity on the hydrodynamic evolution of hot QCD medium, Eur. Phys. J. C **83**, 873 (2023).
[62] G. Mukherjee, D. Dutta, and D. K. Mishra, Conserved number fluctuations under global rotation in a hadron resonance gas model, Eur. Phys. J. C **84**, 258 (2024).
[63] M. N. Chernodub, Inhomogeneous confining-deconfining phases in rotating plasmas, Phys. Rev. D **103**, 054027 (2021).
[64] M. N. Chernodub and S. Gongyo, Effects of rotation and boundaries on chiral symmetry breaking of relativistic fermions, Phys. Rev. D **95**, 096006 (2017).
[65] V. V. Braguta, M. N. Chernodub, A. A. Roenko, and D. A. Sychev, Negative moment of inertia and rotational instability of gluon plasma, Phys. Lett. B **852**, 138604 (2024).
[66] M. N. Chernodub, V. A. Goy, and A. V. Molochkov, Inhomogeneity of a rotating gluon plasma and the Tolman-Ehrenfest law in imaginary time: Lattice results for fast imaginary rotation, Phys. Rev. D **107**, 114502 (2023).
[67] J. Sivardiere, On the analogy between inertial and electromagnetic forces, Eur. J. Phys. **4**, 162 (1983).
[68] B. L. Johnson, Inertial forces and the Hall effect, Am. J. Phys. **68**, 649 (2000).
[69] J. J. Sakurai, Comments on quantum-mechanical interference due to the Earth's rotation, Phys. Rev. D **21**, 2993 (1980).
[70] J. Dey, S. Satapathy, P. Murmu, and S. Ghosh, Shear viscosity and electrical conductivity of the relativistic fluid in the presence of a magnetic field: A massless case, Pramana **95**, 125 (2021).
[71] A. Dash, S. Samanta, J. Dey, U. Gangopadhyaya, S. Ghosh, and V. Roy, Anisotropic transport properties of a hadron resonance gas in a magnetic field, Phys. Rev. D **102**, 016016 (2020).
[72] J. Dey, S. Samanta, S. Ghosh, and S. Satapathy, Quantum expression for the electrical conductivity of massless quark matter and of the hadron resonance gas in the presence of a magnetic field, Phys. Rev. C **106**, 044914 (2022).
[73] A. Bandyopadhyay, S. Ghosh, R. L. S. Farias, J. Dey, and G. Krein, Anisotropic electrical conductivity of magnetized hot quark matter, Phys. Rev. D **102**, 114015 (2020).
[74] J. Dey, S. Satapathy, A. Mishra, S. Paul, and S. Ghosh, From noninteracting to interacting picture of quark–gluon plasma in the presence of a magnetic field and its fluid property, Int. J. Mod. Phys. E **30**, 2150044 (2021).
[75] P. Kalikotay, S. Ghosh, N. Chaudhuri, P. Roy, and S. Sarkar, Medium effects on the electrical and Hall conductivities of a hot and magnetized pion gas, Phys. Rev. D **102**, 076007 (2020).
[76] J. Dey, A. Bandyopadhyay, A. Gupta, N. Pujari, and S. Ghosh, Electrical conductivity of strongly magnetized dense quark matter—Possibility of quantum Hall effect, Nucl. Phys. A **1034**, 122654 (2023).
[77] S. Satapathy, S. Ghosh, and S. Ghosh, Kubo estimation of the electrical conductivity for a hot relativistic fluid in the presence of a magnetic field, Phys. Rev. D **104**, 056030 (2021).
[78] A. Das, H. Mishra, and R. K. Mohapatra, Electrical conductivity and Hall conductivity of a hot and dense hadron gas in a magnetic field: A relaxation time approach, Phys. Rev. D **99**, 094031 (2019).
[79] A. Das, H. Mishra, and R. K. Mohapatra, Electrical conductivity and Hall conductivity of a hot and dense quark gluon plasma in a magnetic field: A quasiparticle approach, Phys. Rev. D **101**, 034027 (2020).
[80] B. Chatterjee, R. Rath, G. Sarwar, and R. Sahoo, Centrality dependence of electrical and Hall conductivity at RHIC and LHC energies for a conformal system, Eur. Phys. J. A **57**, 45 (2021).
[81] K. Hattori and D. Satow, Electrical conductivity of quark-gluon plasma in strong magnetic fields, Phys. Rev. D **94**, 114032 (2016).
[82] K. Hattori, S. Li, D. Satow, and H.-U. Yee, Longitudinal conductivity in strong magnetic field in perturbative QCD: Complete leading order, Phys. Rev. D **95**, 076008 (2017).
[83] S. Satapathy, S. Ghosh, and S. Ghosh, Quantum field theoretical structure of electrical conductivity of cold and dense fermionic matter in the presence of a magnetic field, Phys. Rev. D **106**, 036006 (2022).
[84] C. W. Aung, A. Dwibedi, J. Dey, and S. Ghosh, Effect of Coriolis force on the shear viscosity of quark matter: A nonrelativistic description, Phys. Rev. C **109**, 034913 (2024).
[85] A. Dwibedi, C. W. Aung, J. Dey, and S. Ghosh, Effect of the Coriolis force on the electrical conductivity of quark matter: A nonrelativistic description, Phys. Rev. C **109**, 034914 (2024).
[86] R. Dashen, S.-K. Ma, and H. J. Bernstein, S Matrix formulation of statistical mechanics, Phys. Rev. **187**, 345 (1969).
[87] R. F. Dashen and R. Rajaraman, Narrow resonances in statistical mechanics, Phys. Rev. D **10**, 694 (1974).

[88] F. Karsch, K. Redlich, and A. Tawfik, Thermodynamics at nonzero baryon number density: A comparison of lattice and hadron resonance gas model calculations, Phys. Lett. B **571**, 67 (2003).

[89] P. Braun-Munzinger, V. Koch, T. Schäfer, and J. Stachel, Properties of hot and dense matter from relativistic heavy ion collisions, Phys. Rep. **621**, 76 (2016).

[90] V. V. Begun, M. I. Gorenstein, M. Hauer, V. P. Konchakovski, and O. S. Zozulya, Multiplicity fluctuations in hadron-resonance gas, Phys. Rev. C **74**, 044903 (2006).

[91] M. Nahrgang, M. Bluhm, P. Alba, R. Bellwied, and C. Ratti, Impact of resonance regeneration and decay on the net-proton fluctuations in a hadron resonance gas, Eur. Phys. J. C **75**, 573 (2015).

[92] A. Bazavov *et al.* (HotQCD Collaboration), Fluctuations and correlations of net baryon number, electric charge, and strangeness: A comparison of lattice QCD results with the hadron resonance gas model, Phys. Rev. D **86**, 034509 (2012).

[93] A. Bhattacharyya, S. Das, S. K. Ghosh, R. Ray, and S. Samanta, Fluctuations and correlations of conserved charges in an excluded volume hadron resonance gas model, Phys. Rev. C **90**, 034909 (2014).

[94] A. Chatterjee, S. Chatterjee, T. K. Nayak, and N. R. Sahoo, Diagonal and off-diagonal susceptibilities of conserved quantities in relativistic heavy-ion collisions, J. Phys. G **43**, 125103 (2016).

[95] M. I. Gorenstein, M. Hauer, and O. N. Moroz, Viscosity in the excluded volume hadron gas model, Phys. Rev. C **77**, 024911 (2008).

[96] J. Noronha-Hostler, J. Noronha, and C. Greiner, Hadron mass spectrum and the shear viscosity to entropy density ratio of hot hadronic matter, Phys. Rev. C **86**, 024913 (2012).

[97] S. K. Tiwari, P. K. Srivastava, and C. P. Singh, Description of hot and dense hadron gas properties in a new excluded-volume model, Phys. Rev. C **85**, 014908 (2012).

[98] K. K. Pradhan, D. Sahu, R. Scaria, and R. Sahoo, Conductivity, diffusivity, and violation of the Wiedemann-Franz law in a hadron resonance gas with van der Waals interactions, Phys. Rev. C **107**, 014910 (2023).

[99] J. Noronha-Hostler, J. Noronha, and C. Greiner, Transport coefficients of hadronic matter near T_c, Phys. Rev. Lett. **103**, 172302 (2009).

[100] G. P. Kadam and H. Mishra, Bulk and shear viscosities of hot and dense hadron gas, Nucl. Phys. A **934**, 133 (2015).

[101] H.-X. Zhang, J.-W. Kang, and B.-W. Zhang, In-medium effect on the thermodynamics and transport coefficients in the van der Waals hadron resonance gas, Phys. Rev. D **101**, 114033 (2020).

[102] S. Samanta, S. Ghosh, and B. Mohanty, Finite size effect of hadronic matter on its transport coefficients, J. Phys. G **45**, 075101 (2018).

[103] S. Ghosh, S. Samanta, S. Ghosh, and H. Mishra, Viscosity calculations from hadron resonance gas model: Finite size effect, Int. J. Mod. Phys. E **28**, 1950036 (2019).

[104] S. Ghosh, S. Ghosh, and S. Bhattacharyya, Phenomenological bound on the viscosity of the hadron resonance gas, Phys. Rev. C **98**, 045202 (2018).

[105] G. S. Rocha and G. S. Denicol, Transport coefficients of transient hydrodynamics for the hadron-resonance gas and thermal-mass quasiparticle models, Phys. Rev. D **109**, 096011 (2024).

[106] M. N. Chernodub and S. Gongyo, Interacting fermions in rotation: Chiral symmetry restoration, moment of inertia and thermodynamics, J. High Energy Phys. 01 (2017) 136.

[107] Y. Fujimoto, K. Fukushima, and Y. Hidaka, Deconfining phase boundary of rapidly rotating hot and dense matter and analysis of moment of inertia, Phys. Lett. B **816**, 136184 (2021).

[108] S. Ebihara, K. Fukushima, and K. Mameda, Boundary effects and gapped dispersion in rotating fermionic matter, Phys. Lett. B **764**, 94 (2017).

[109] M. N. Chernodub and S. Gongyo, Edge states and thermodynamics of rotating relativistic fermions under magnetic field, Phys. Rev. D **96**, 096014 (2017).

[110] J. I. Kapusta, E. Rrapaj, and S. Rudaz, Relaxation time for strange quark spin in rotating quark-gluon plasma, Phys. Rev. C **101**, 024907 (2020).

[111] C. Misner, K. Thorne, J. Wheeler, and D. Kaiser, *Gravitation* (Princeton University Press, Princeton, NJ, 2017).

[112] B. Schutz, *A First Course in General Relativity* (Cambridge University Press, Cambridge, UK, 2009).

[113] C. Cercignani and G. M. Kremer, Riemann spaces and general relativity, in *The Relativistic Boltzmann Equation: Theory and Applications* (Birkhäuser Basel, Basel, 2002), pp. 291–325.

[114] C. Cercignani and G. M. Kremer, Tensor calculus in general coordinates, in *The Relativistic Boltzmann Equation: Theory and Applications* (Birkhäuser Basel, Basel, 2002), pp. 271–290.

[115] H. Goldstein, *Classical Mechanics* (Pearson Education India, Delhi, 2011).

[116] D. Kleppner and R. Kolenkow, *An Introduction to Mechanics* (Cambridge University Press, Cambridge, UK, 2014).

[117] G. M. Kremer, Relativistic gas in a Schwarzschild metric, J. Stat. Mech. (2013) P04016.

[118] C. Cercignani and G. M. Kremer, Boltzmann equation in gravitational fields, in *The Relativistic Boltzmann Equation: Theory and Applications* (Birkhäuser Basel, Basel, 2002), pp. 327–346.

[119] G. M. Kremer, The Boltzmann equation in special and general relativity, AIP Conf. Proc. **1501**, 160 (2012).

[120] G. M. Kremer, Diffusion of relativistic gas mixtures in gravitational fields, Physica A **393**, 76 (2014).

[121] G. M. Kremer, Theory and applications of the relativistic Boltzmann equation, Int. J. Geom. Methods Mod. Phys. **11**, 1460005 (2014).

[122] V. Moratto and G. M. Kremer, Mixtures of relativistic gases in gravitational fields: Combined Chapman-Enskog and Grad method and the Onsager relations, Phys. Rev. E **91**, 052139 (2015).

[123] F. Debbasch and W. van Leeuwen, General relativistic Boltzmann equation, I: Covariant treatment, Physica A **388**, 1079 (2009).

[124] F. Debbasch and W. van Leeuwen, General relativistic Boltzmann equation, II: Manifestly covariant treatment, Physica A **388**, 1818 (2009).

[125] P. Romatschke, Relativistic (lattice) Boltzmann equation with non-ideal equation of state, Phys. Rev. D **85**, 065012 (2012).

[126] C. Amsler *et al.* (Particle Data Group), Review of particle physics, Phys. Lett. B **667**, 1 (2008).

[127] W. Cassing, O. Linnyk, T. Steinert, and V. Ozvenchuk, Electrical conductivity of hot QCD matter, Phys. Rev. Lett. **110**, 182301 (2013).

[128] R. Marty, E. Bratkovskaya, W. Cassing, J. Aichelin, and H. Berrehrah, Transport coefficients from the Nambu-Jona-Lasinio model for $SU(3)_f$, Phys. Rev. C **88**, 045204 (2013).

[129] D. Fernandez-Fraile and A. Gomez Nicola, The electrical conductivity of a pion gas, Phys. Rev. D **73**, 045025 (2006).

[130] H.-T. Ding, A. Francis, O. Kaczmarek, F. Karsch, E. Laermann, and W. Soeldner, Thermal dilepton rate and electrical conductivity: An analysis of vector current correlation functions in quenched lattice QCD, Phys. Rev. D **83**, 034504 (2011).

[131] G. Aarts, C. Allton, J. Foley, S. Hands, and S. Kim, Spectral functions at small energies and the electrical conductivity in hot quenched lattice QCD, Phys. Rev. Lett. **99**, 022002 (2007).

[132] P. V. Buividovich, M. N. Chernodub, D. E. Kharzeev, T. Kalaydzhyan, E. V. Luschevskaya, and M. I. Polikarpov, Magnetic-field-induced insulator-conductor transition in $SU(2)$ quenched lattice gauge theory, Phys. Rev. Lett. **105**, 132001 (2010).

[133] Y. Burnier and M. Laine, Towards flavour-diffusion coefficient and electrical conductivity without ultraviolet contamination, Eur. Phys. J. C **72**, 1902 (2012).

[134] S. Gupta, The electrical conductivity and soft photon emissivity of the QCD plasma, Phys. Lett. B **597**, 57 (2004).

[135] B. B. Brandt, A. Francis, H. B. Meyer, and H. Wittig, Thermal correlators in the ρ channel of two-flavor QCD, J. High Energy Phys. 03 (2013) 100.

[136] A. Amato, G. Aarts, C. Allton, P. Giudice, S. Hands, and J.-I. Skullerud, Electrical conductivity of the quark-gluon plasma across the deconfinement transition, Phys. Rev. Lett. **111**, 172001 (2013).

[137] Y. Yin, Electrical conductivity of the quark-gluon plasma and soft photon spectrum in heavy-ion collisions, Phys. Rev. C **90**, 044903 (2014).

[138] A. Puglisi, S. Plumari, and V. Greco, Electric conductivity from the solution of the relativistic Boltzmann equation, Phys. Rev. D **90**, 114009 (2014).

[139] M. Greif, I. Bouras, C. Greiner, and Z. Xu, Electric conductivity of the quark-gluon plasma investigated using a perturbative QCD based parton cascade, Phys. Rev. D **90**, 094014 (2014).

[140] S. I. Finazzo and J. Noronha, Holographic calculation of the electric conductivity of the strongly coupled quark-gluon plasma near the deconfinement transition, Phys. Rev. D **89**, 106008 (2014).

[141] C.-H. Lee and I. Zahed, Electromagnetic radiation in hot QCD matter: Rates, electric conductivity, flavor susceptibility, and diffusion, Phys. Rev. C **90**, 025204 (2014).

[142] Y. B. Ivanov and A. A. Soldatov, Vorticity in heavy-ion collisions at the JINR nuclotron-based ion collider facility, Phys. Rev. C **95**, 054915 (2017).